

Impact of dendritic non-linearities on the computational capabilities of neurons

Clarissa Lauditi,¹ Enrico M. Malatesta,² Fabrizio Pittorino,^{2,3}
Carlo Baldassi,² Nicolas Brunel,^{2,4} and Riccardo Zecchina²

¹*Department of Applied Math, John A. Paulson School of Engineering and Applied Sciences,
Harvard University, 02138 Cambridge, MA, USA*

²*Department of Computing Sciences and Bocconi Institute for Data
Science and Analytics (BIDSA), Bocconi University, 20136 Milano, Italy*

³*Department of Electronics, Information and Bioengineering, Politecnico di Milano, 20133 Milano, Italy*

⁴*Departments of Neurobiology and Physics, Duke University,
Durham, North Carolina, United States of America*

Multiple neurophysiological experiments have shown that dendritic non-linearities can have a strong influence on synaptic input integration. In this work we model a single neuron as a two-layer computational unit with non-overlapping sign-constrained synaptic weights and a biologically plausible form of dendritic non-linearity, which is analytically tractable using statistical physics methods. Using both analytical and numerical tools, we demonstrate several key computational advantages of non-linear dendritic integration with respect to models with linear synaptic integration. We find that the dendritic non-linearity concurrently enhances the number of possible learned input-output associations and the learning velocity, and we characterize how capacity and learning speed depend on the implemented non-linearity and the levels of dendritic and somatic inhibition. We find that experimentally observed connection probabilities naturally emerge in neurons with sign-constrained synapses as a consequence of non-linear dendritic integration, while in models with linear integration, an additional robustness parameter must be introduced in order to reproduce realistic connection probabilities. Non-linearly induced sparsity comes with a second central advantage for neuronal information processing, i.e. input and synaptic noise robustness. By testing our model on standard real-world benchmark datasets inspired by deep learning practice, we observe empirically that the non-linearity provides an enhancement in generalization performance, showing that it enables to capture more complex input/output relations.

Understanding the computational capabilities of single neurons is among the most fundamental open problems in neuroscience. A long-standing question concerns the role of dendrites in shaping neuronal information processing. In the simplest scenario, dendrites are devices that sum synaptic inputs linearly, propagating a dot product of a vector of pre-synaptic activity with a vector of synaptic weights to the axon initial segment, where a thresholding operation is applied to decide whether the neuron emits an action potential or not. In this view, neurons are analogous to simple perceptrons, whose learning capabilities have been studied extensively (e.g. [1–4]).

However, this view ignores the presence of active currents in dendrites, that can potentially lead to non-linear integration of synaptic inputs (for reviews, see e.g. [5–7]). These non-linearities are due to various types of voltage-gated ionic currents, such as NMDA receptor mediated synaptic currents [8, 9], calcium currents [10, 11], or sodium currents [12].

In cortical pyramidal neurons, in particular, it has been shown [13] that inputs to a single dendritic branch sum in a strongly non-linear fashion, while inputs to distinct dendritic branches sum linearly.

These results have led to the idea that neurons could be better described by multi-layer devices than the standard perceptron [14–20].

Given the non-overlapping tree-like morphology of dendrites and the non-linear integration of synaptic inputs

pertaining to the same dendritic branch, a natural choice is to model single neurons as a particular type of a two-layer neural network called a tree committee machine. The computational properties of this neural architecture have been extensively studied in the statistical physics literature. In the early works from the 1990s [21, 22], it has been shown that the storage capacity of tree committee machines increases with the size of the hidden layer K . In the case of the sign non-linearity $g(x) \equiv \text{sign}(x)$, the maximal number of random input/output associations that can be learned scales as $P_c = \alpha_c(K)N$ where $\alpha_c(K) \propto \sqrt{\ln K}$, and N is the number of inputs [23]. Recently, it was pointed out that these results are valid only for activation functions presenting a discontinuity at the origin [24, 25]. In particular, in the case of the Rectified Linear Unit (ReLU) non-linearity, an activation function commonly used in machine learning, the capacity of the tree committee machine remains finite as the size of the hidden layer K goes to infinity [24]. Moreover, most of the non-linearities used in machine learning enhance learning by smoothing the corresponding loss landscape and inducing flatter and more robust minima that are attractive for gradient-based algorithms such as Stochastic Gradient Descent (SGD) [24, 26–29].

The aforementioned studies on the tree-committee machine from the statistical physics/machine learning community are typically performed without including biological constraints on the excitatory/inhibitory nature

of synaptic weights (i.e. constraints on their sign), and without considering the specific dendritic non-linearities that are observed experimentally. Given that multilayer networks are well known to have more powerful representation and generalization capabilities than single layer ones, as mathematically shown in early works on approximation capabilities of multilayer neural networks [30], a natural question is to what extent dendritic non-linearities enhance the computational capabilities of single biological neurons.

Here, we set out to study the computational capabilities of a single neuron model with dendritic branches implementing experimentally observed non-linear integration and with sign-constrained positive synapses modelling excitatory connectivity, while inhibitory inputs are incorporated into dendritic and somatic thresholds. We show that on this two-layer sign-constrained analytically tractable neuron model, a biologically motivated saturating non-linearity has the effect of enhancing single neuron computational capabilities along several biologically relevant axes, such as the number of possible stored input-output associations (capacity), training speed, noise robustness and generalization to unseen inputs, while also being able to reproduce the experimentally observed synaptic weight distribution and sparsity. Interestingly, while in standard perceptrons with constrained synapses, sparse synaptic input connectivity can only be obtained when a robustness parameter is introduced [31, 32], dendritic non-linear input integration lead to high sparsity even in the absence of any robustness constraint.

I. SINGLE NEURON MODEL

We consider a single neuron model that transforms N binary synaptic inputs $\xi_i = \{0, 1\}^N$ into a binary output $\hat{\sigma} = \{0, 1\}$. In the standard perceptron model, the neuronal output is

$$\hat{\sigma} = \Theta \left(\sum_{i=1}^N W_i \xi_i - T \right) \quad (1)$$

where Θ is the Heaviside function, \mathbf{W} is a vector of synaptic weights, typically optimized by a learning process, and T is a threshold.

Here, motivated by experiments that have revealed significant non-linearities in the summation of inputs within single dendritic branches, but not across branches [6, 8, 13], we consider a generalization of the perceptron model with K dendritic branches, and non-linear summation of inputs within each dendritic branch (see Fig. 1). In this model, the neuronal output $\hat{\sigma}$ is

$$\hat{\sigma} = \Theta(\Delta) \quad (2a)$$

$$\Delta = \frac{1}{\sqrt{K}} \sum_{l=1}^K g(\lambda_l) - \sqrt{K} \theta_s \quad (2b)$$

$$\lambda_l = \sqrt{\frac{K}{N}} \sum_{i=1}^{N/K} W_{li} \xi_{li} - \sqrt{\frac{N}{K}} \theta_d \quad (2c)$$

where Δ is the total input to the soma, proportional to the sum of the outputs of all dendritic branches; g is a non-linear function describing the dendritic non-linearity; λ_l is the total input to dendritic branch l , which is a linear sum of inputs to this branch $\xi_{li} \in \{0, 1\}^{N/K}$, weighted by synaptic efficacies W_{li} ; θ_s is a somatic threshold and θ_d is a dendritic threshold. Notice that this model corresponds to a feedforward network with a layer of hidden units endowed with a non-linear transfer function, corresponding to the dendritic branches, and a fixed output summation layer.

Constraints on weights, excitation and inhibition

The efficacy of real synapses is constrained by the identity of the pre-synaptic neuron. Synaptic weights are non-negative when the pre-synaptic neuron is excitatory (glutamatergic), while they are non-positive when the pre-synaptic neuron is inhibitory (GABAergic). Here, we consider for simplicity a scenario in which only the excitatory weights are modeled explicitly and are plastic. Inhibitory synapses are assumed not to be affected by learning, and are lumped together in the two thresholds, θ_d and θ_s , describing inhibitory synapses onto dendritic branches and the perisomatic region, respectively. Thus, all synaptic weights W_{li} in Eq. (2c) obey the constraint $W_{li} \geq 0$.

Dendritic non-linearity

Experiments in neocortical pyramidal cells have indicated that the dendritic output is roughly linear at low stimulation intensities, and that it then increases in a strongly non-linear fashion beyond a threshold, before saturating [13].

To capture quantitatively these findings, we consider the following dendritic non-linear transfer function

$$g_{\text{polsky}}(x) = \begin{cases} \max(0, x) & x < x_{\min} \\ \frac{2(1-x_{\min})}{1+e^{-\gamma(x-x_{\min})}} - 1 + 2x_{\min} & x \geq x_{\min} \end{cases} \quad (3)$$

where x_{\min} is a dendritic non-linearity threshold, and γ describes the strength of the non-linearity. We refer to this non-linearity as the Polsky transfer function. It is plotted in the inset of Fig. 1. In the following we use $x_{\min} = 0.33$ and $\gamma = 15$, which provide a good approximation of the non-linear function measured in [13], see Methods for a discussion on the biologically realistic values of the parameters. Notice that this transfer function interpolates between the ReLU non-linearity

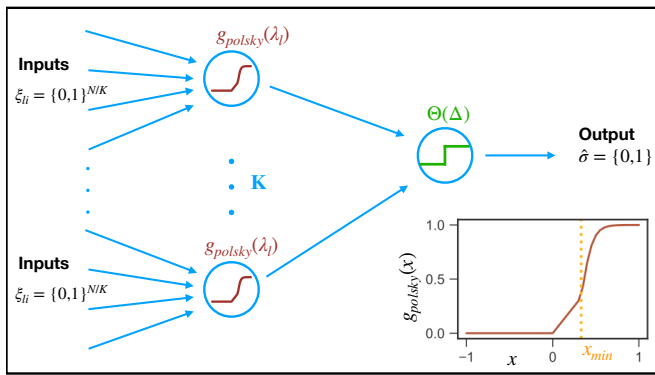


Figure 1. Single-neuron model with dendritic non-linearities. The neuron has K dendritic branches as in (2a). Synaptic inputs to each dendritic branch are summed linearly and then processed through a dendritic non-linearity depicted in the inset. The outputs of the dendritic branches are then summed linearly and compared to a somatic threshold.

(when $x_{\min} \rightarrow \infty$) and the step non-linearity, obtained for $x_{\min} = 0$, $\gamma \rightarrow \infty$. Note also that in the experiments of ref. [13], only excitatory inputs are considered, and consequently only the positive side of the dendritic non-linearity is probed. On the negative side, we take for simplicity g to be equal to zero. This scenario can be thought of capturing in a simplified way shunting inhibition.

Scaling of inputs and thresholds

Pyramidal cells have on the order of 10,000 synaptic inputs [33, 34], scattered along tens to hundreds dendritic branches [35]. In this limit, assuming synaptic weights and thresholds are of order 1 ($W_{ij} \sim \theta_d \sim \mathcal{O}(1)$), inputs to dendritic branches scale as N/K due to the sign constraints on the weights, with fluctuations of order $\sqrt{N/K}$ around the mean. To obtain a well-defined limit with finite means and variances, the dendritic threshold should balance the mean inputs, and the difference should be rescaled by $\sqrt{K/N}$. Likewise, at the somatic level, the somatic threshold should cancel the average somatic input, and the difference should be rescaled by $1/\sqrt{K}$. These considerations explain the scalings in Eqs. (2a-2c).

Learning tasks

We consider first a standard classification task with the objective of learning a dataset $\mathcal{D} = \{\xi^\mu, \sigma^\mu\}_{\mu=1}^P$ composed of $P = \alpha N$ binary random input patterns ξ_{li}^μ that are i.i.d. Bernoulli variables with $P(\xi_{li}^\mu = 1) = f_{\text{in}}$ (input coding level) and labels σ^μ that are i.i.d. Bernoulli variables with $P(\sigma^\mu = 1) = f_{\text{out}}$ (output coding level). The task of the neuron is to correctly classify all input

patterns, i.e. produce the correct output $\hat{\sigma} = \sigma^\mu$ when input ξ^μ is presented. These input/output associations can be learned by progressively modifying the synaptic weights, either by optimizing directly the number of errors or some surrogate loss functions. This classification task (often called "storage problem" in the literature) has been studied extensively for the perceptron architecture [3, 36], including also cases with sign-constrained weights [32, 37, 38]. It has also been studied in tree committee machines with sign non-linearity on the hidden units [22, 23, 39], as well as more recently with generic non-linearity [24, 25]. On the numerical side only, we also study classical benchmark classification tasks in machine learning, providing realistic correlated datasets, such as MNIST [40], Fashion-MNIST [41] and CIFAR-10 [42].

Learning algorithms

To evaluate the computational performance of the two-layer non-linear neuron described in (2), which is endowed with K dendritic branches and the transfer function defined in (3), and compare it with the linear neuron defined in (1) from an algorithmic standpoint, we develop algorithms capable of learning with sign-constrained synapses. We then proceed to examine their behavior on various paradigmatic learning tasks. These algorithms are modified versions of Stochastic Gradient Descent (SGD) and Least Action Learning (LAL) [22, 27], as detailed in the Methods section - see Algo. 1 for SGD and Algo. 2 for LAL. Due to the positive nature of excitatory synapses, whenever the learning rule leads them to become negative, they are instantaneously set to zero. It is worth noting that for the one-layer linear neuron model, the LAL algorithm reduces to the usual perceptron update rule [4] with a hard threshold on negative synapses, whose behavior has been studied in [32, 43]. Importantly, the definition of the two models, particularly the tree-like nature of the dendritic layer of the non-linear neuron, naturally allows for their comparison at the same number of synaptic parameters, ensuring that computational improvements are exclusively attributable to their architectural and linear/nonlinear properties.

II. STORAGE CAPACITY

Analytical methods

To investigate the properties of our single neuron model in the storage setting, one can make use of asymptotic methods from statistical physics [4, 44]. Given a density of patterns α , the uniform probability measure over all configurations classifying the patterns in \mathcal{D} (or *solutions* to the learning problem) can be expressed,

apart from a normalization factor, as

$$\mathbb{X}_{\mathcal{D}}(\mathbf{W}) = \prod_{\mu=1}^P \Theta[(2\sigma^{\mu} - 1)\Delta^{\mu}(\mathbf{W}; \theta_d, \theta_s) - \kappa] \quad (4)$$

where Δ^{μ} is the somatic input defined in (2b) and σ^{μ} is the correct label for input μ . The parameter κ is a margin that imposes a certain degree of robustness on the learned \mathbf{W} . Exploiting self-averaging properties, the typical Gibbs entropy, which is the logarithm of the volume of solutions can be obtained by taking the average $\langle \cdot \rangle_{\mathcal{D}}$ over the quenched disorder induced by the random realization of patterns and labels

$$\phi = \lim_{N, K, P \rightarrow \infty} \frac{1}{N} \left\langle \ln \int d\mu(\mathbf{W}) \mathbb{X}_{\mathcal{D}}(\mathbf{W}) \right\rangle_{\mathcal{D}} \quad (5)$$

In (5), $\int d\mu(\mathbf{W}) \bullet \equiv \int_0^{\infty} \prod_i dW_{li} \bullet$ is the integral over the prior weight measure, with the integration bounds reflecting the constraint over the weights. In order to compute the average $\langle \cdot \rangle_{\mathcal{D}}$ in (5), one can resort to the Replica Method in the Replica Symmetric (RS) approximation [45]. We refer to the Methods section for a brief description of the analytical methods and to the Supplementary Information (SI) for more detailed derivations.

Pyramidal cells receive roughly 10000 synaptic inputs, which are distributed across several dozen to several hundred dendritic branches [33–35]. We therefore considered the limit of large number K of dendritic branches in our analytical calculations. At the same time, however we consider the regime where K is small compared to the total number of synapses N , i.e. $K/N \rightarrow 0$. This is not only a realistic assumption, but it also allows us to reduce the computational complexity of the analytical calculations which are valid for a generic non-linearity (see Methods).

As we show in the SI, computing the entropy (5) in the large N and K limit, in turn, gives access to several physical observables of interest, namely the critical capacity and the distribution of synaptic weights.

Critical capacity

The randomness of the labels in the dataset, does not make the task learnable for any value of the constrained density α . Indeed, in the large N limit, there exists a sharp threshold α_c for the probability of finding a solution to the learning problem. For $\alpha < \alpha_c$ this probability is 1, meaning that there an exponential number of synaptic weight configurations that are able to classify the inputs correctly; at $\alpha = \alpha_c$ the probability of finding a solutions drops abruptly to zero. For $\alpha > \alpha_c$ the complexity of the model is therefore no longer sufficient to classify the activity patterns. α_c can be thought as a measure of expressivity of our single neuron model.

At α_c the typical overlap q between pair of solutions extracted from the Gibbs measure (4) tends towards the typical squared norm Q of solutions. We have therefore expanded the entropy in terms of the variable $dq \equiv Q - q$. We report in the SI the technical details of how α_c can be computed from this scaling, for a given value of the external parameters $\theta_d, \theta_s, f_{\text{in}}, f_{\text{out}}, \kappa$ and for a generic activation function g .

In the case of a linear activation function (i.e. $g(x) \equiv x$), our model is equivalent to the one-layer neuron model whose activity is based on a thresholding operation θ_d applied to the soma. In this case we recover the results on the critical capacity α_c^{perc} [32, 37, 38, 43]. If the margin $\kappa = 0$ it has been shown in [38] that the capacity is independent on θ_d ; in particular, for $f_{\text{in}} = f_{\text{out}} = 0.5$, $\alpha_c^{\text{perc}} = 1$.

This is not true in the case of the two-layer neuron model, in which changing the dendritic threshold *strongly* alters the expressivity of the model. In the upper left panel of Fig. 2 we show the plot of the critical capacity of our two-layer neuron model as function of θ_d for different types of dendritic non-linearities, namely ReLU, a “saturating” ReLU function $\min(\max(0, x), 1)$, and Polsky as in (3). For comparison purposes we also plot the critical capacity of the one-layer neuron model. As the figure shows, the storage capacity of the model is greatly enhanced by the presence of the non-linearity. As shown analytically in the SI, in the limit $\theta_d \rightarrow 0$, the two-layer neuron models becomes equivalent to the one-layer perceptron model. When θ_d increases, all models with non-linear integration increase their capacity, but in a strongly non-linearity-dependent way. With a non-saturating non-linearity such as ReLU, the increase in capacity is logarithmic in θ_d , and it is much smaller than with saturating non-linearities where the capacity increases linearly with θ_d . Finally, the model with Polsky non-linearity outperforms the saturating ReLU function, thanks to the additional non-linear region for $x > x_{\text{min}}$.

The behaviour of α_c as a function of θ_d can be understood through an analysis of the shape of the distribution of dendritic preactivation, which we show in the SI to be a Gaussian with a mean and variance that are functions of the norm of the weights Q , and the input coding level f_{in} . We show the shape of the dendritic preactivation for the Polsky activation in the inset of the upper left panel of Fig. 2 for several values of θ_d . If θ_d is small, the distribution is peaked in a range where the Polsky activation behaves linearly; therefore, the model cannot fully exploit the non-linearity and behaves as a one-layer model. On the contrary, by increasing θ_d , the dendritic preactivation distribution widens towards the region where the Polsky activation saturates; if one keeps increasing θ_d the weight of the active region before saturation becomes negligible. In this limit, we expect the critical capacity to diverge, since the Polsky activation becomes equivalent to the Heaviside theta activation.

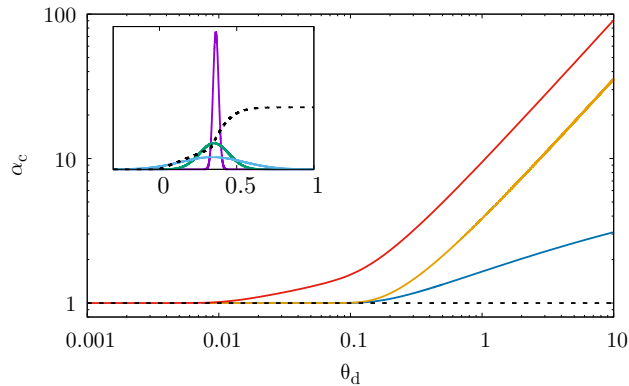
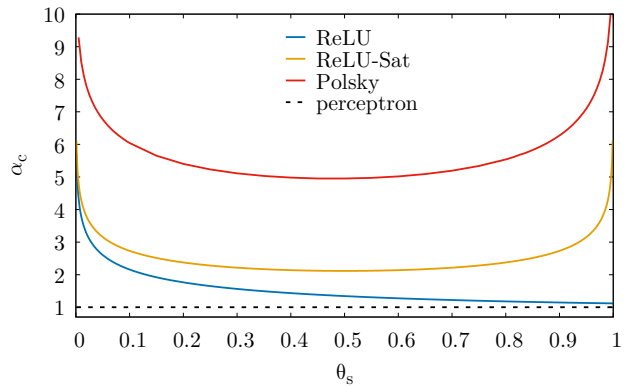
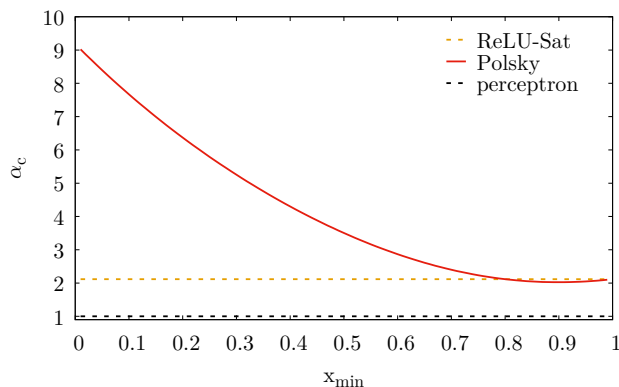
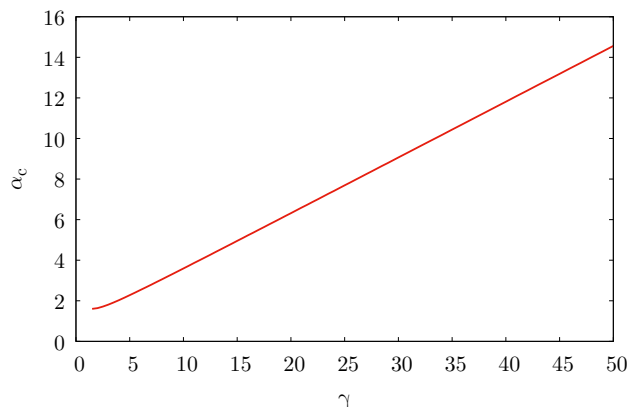
(a) $\kappa = 0$, $f_{\text{in}} = f_{\text{out}} = 0.5$ and $\theta_s = 0.5$, $x_{\text{min}} = 0.33$, $\gamma = 15$.(b) $\kappa = 0$, $f_{\text{in}} = f_{\text{out}} = 0.5$ and $\theta_d = 0.5$, $x_{\text{min}} = 0.33$, $\gamma = 15$.(c) $\kappa = 0$, $f_{\text{in}} = f_{\text{out}} = 0.5$ and $\theta_s = \theta_d = 0.5$, $\gamma = 15$.(d) $\kappa = 0$, $f_{\text{in}} = f_{\text{out}} = 0.5$ and $\theta_s = \theta_d = 0.5$, $x_{\text{min}} = 0.33$.

Figure 2. Critical capacities α_c for ReLU, saturating ReLU and Polsky non-linearities as a function of the dendritic threshold θ_d (upper left panel), the somatic threshold (upper right panel). The dashed black line represents the case of the one-layer neuron model, where the critical capacity $\alpha_c^{\text{perc}} = 1$. In the inset of the upper left panel we also show the plot of the distribution of the preactivations for $\theta_d = 0.01, 0.05$ and 0.1 (respectively violet, green and cyan curves); we also plot with the dashed black line the Polsky activation to better show the extent to which the entire non-linearity is exploited for that value of θ_d . In the bottom panels we plot α_c as a function of the parameters of the Polsky activation x_{min} (left panel) and γ (right). In the captions of the panel we show the value of the fixed external parameters.

The capacity α_c also strongly depends on the somatic threshold θ_s , as shown in the upper right panel of Fig. 2. In the bottom panels of Fig. 2 we show how the capacity of the network with a Polsky non-linearity depends on the choice of its parameters x_{min} and γ . The critical capacity increases both decreasing x_{min} or increasing γ , as in this case the non-linearity is closer to the Heaviside theta function. When $x_{\text{min}} = 1$, the Polsky non-linearity effectively reduces to the "saturating" ReLU function, and so the capacity of the two models coincide in this limit.

Notice that the estimation of the critical capacity that we have done is based on the Replica Symmetric (RS) ansatz; in general since the model we are analyzing is non-convex, the RS ansatz is thought to be only an upper bound to the true result. In order to get more precise results on the critical capacity, one needs to resort to the Replica Symmetry Breaking ansatz (RSB) [46].

1RSB corrections to the critical capacity estimation has been computed in one and two layer non-convex neural network models with no constraint on the sign of the weights [22, 24, 25, 47, 48]. Recently, the exact capacity of infinitely wide tree committee machines and perceptrons with negative stability has been computed using a full-RSB ansatz [49]. For our two-layer neuron model, computing 1RSB effects on the storage capacity is technically very challenging. Note also that our calculations are done in the $K \rightarrow \infty$ limit. Networks with finite K are expected to have a capacity of at most $16\sqrt{\log(K)}/\pi$, the asymptotic behavior of committee machine with step function non-linearity and no constraints on weights [23]. For values of K in the range 30-100, this leads to upper bounds in the range 6-7, far below the large K estimates of the capacity shown in Fig. 2 for large θ_d . Thus, the benefits of the specific Polsky non-linearity are expected

to be the strongest in an intermediate region of values of θ_d , x and γ .

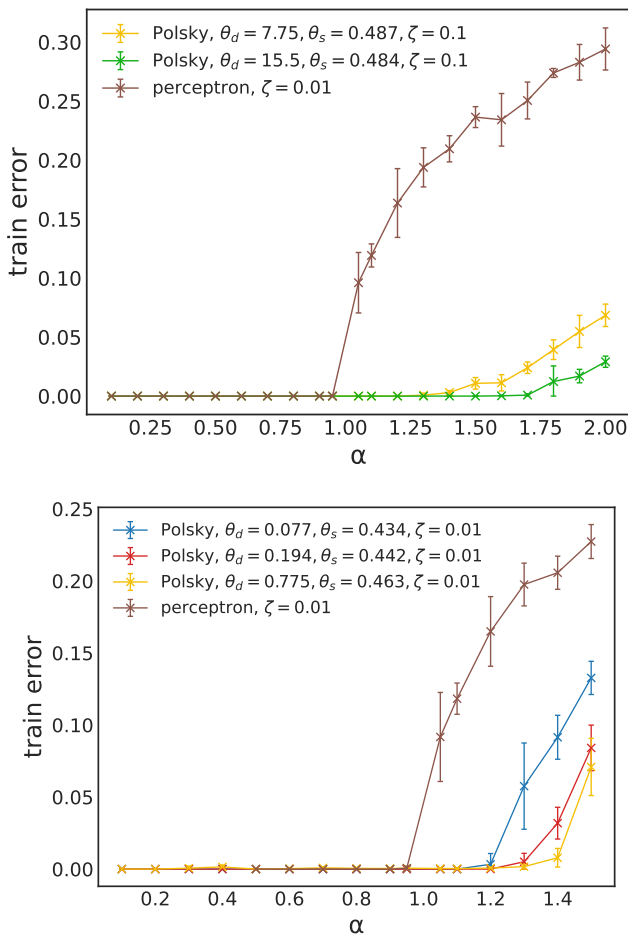


Figure 3. **Fraction of misclassified patterns on the training set** as a function of the total fraction of patterns $\alpha = \frac{P}{N}$ for the non-linear neuron compared with the linear one. The upper panel shows the results for the LAL algorithm (Algo 2), while the lower panel presents the results for SGD (Algo. 1). The curves show different representative values of the dendritic and somatic thresholds θ_d and θ_s . For both neuron models the number of synapses (equivalently, the input size) is $N = 999$, the number of dendritic branches for the non-linear neuron is $K = 27$, and each curve is averaged over 10 realizations of the initial conditions. Note that the non-linear neuron achieves capacities greater than the maximal capacity of the linear perceptron model, which is $\alpha_c^{perc} = 1$. The optimal learning rate for both the linear and non-linear neurons is $\zeta = 0.01$ when using SGD. For LAL, the optimal learning rate is $\zeta = 0.01$ for the linear model and $\zeta = 0.1$ for the non-linear neuron.

Algorithmic capacity and learning speed

In the previous section, we computed an upper bound for the maximal capacity using a RS calculation. We now

turn to the question of the capacity of specific learning algorithms, and to the question of the speed of learning. We use two different algorithms, SGD and LAL (see Methods for details of both algorithms). It is important to note that, unlike the linear neuron model, the optimization problem in the two-layer non-linear neuron is highly non-convex, and there is no guarantee that algorithms can reach the critical capacity, similar to results concerning binary ± 1 weights models [26, 50, 51].

In Fig. 3, we report the final training error after training with SGD (Algo.1) and LAL (Algo. 2) as a function of the control parameter $\alpha = \frac{P}{N}$ (i.e., the density of input patterns) for both the linear and non-linear neuron models. The upper panel corresponds to SGD, while the lower panel corresponds to LAL. Fig. 4 depicts the training error as a function of the training time for both SGD (upper panel) and LAL (lower panel). For both algorithms, we select the optimal hyper-parameters that maximize the algorithmic capacity and training speed using a grid search procedure (see Methods). It is worth noting that, at fixed values of the dendritic and somatic thresholds θ_d and θ_s , the SGD algorithm has two hyper-parameters: the learning rate ζ and the cross-entropy parameter γ_{ce} . In contrast, the LAL algorithm has a single hyper-parameter, i.e., the learning rate ζ . The Methods section provides an in-depth discussion of algorithmic implementations and hyper-parameter selection for both the algorithmic capacity evaluation and the training speed.

As Fig. 3 shows that the neuron with non-linear dendritic integration is able to reach algorithmic capacities that are larger than the maximum one achievable by the linear model, i.e., $\alpha_c^{perc} = 1$, both with the SGD and LAL algorithms. Since the comparison between the two neuron models is performed at the same number of parameters (the number of synapses is $N = 999$ in both cases), the improvement in performance is solely attributable to dendritic nonlinearities. It is worth noting that in the linear model, both algorithms can reach $\alpha_{alg} = \alpha_c^{perc} = 1$ due to the convexity of the problem. Concurrently, as reported in Fig. 4, we find that the non-linear neuron requires fewer steps to learn the training set compared to its linear counterpart, both with the SGD and LAL algorithms.

As shown in Fig. 5, the algorithmic capacity of LAL monotonically increases with the dendritic threshold θ_d . This is because higher θ_d values lead to pre-activations that are more likely to be in the asymptotic range of the Polsky transfer function in $\pm\infty$ (i.e. 0 and 1), which is well-suited for the LAL algorithm that was developed for this scenario [22, 27]. In contrast, SGD exhibits non-monotonic behavior, with an optimal θ_d value around 1, corresponding to the active range of the g_{polsky} transfer function. The non-monotonic behavior of SGD's algorithmic capacity with respect to the dendritic threshold θ_d can be understood as follows. At low θ_d values, the

pre-activation variance is small and in the linear part of the Polsky transfer function, recovering the Perceptron behavior. Conversely, at higher θ_d values, the step-like nature of the Polsky function becomes more relevant. To fully exploit the Polsky function's expressivity in gradient evaluation, an optimal $\theta_d \sim 1$ should be used. The maximal algorithmic capacity of the LAL algorithm adapted for positive weights and binary $\{0, 1\}$ patterns (Algo. 2), reached at high values of the dendritic threshold θ_d , is higher compared to the positive-weight SGD variant (Algo. 1). However, this does not hold for the entire θ_d -range; in particular, SGD compares favorably to LAL at small θ_d values.

Despite the fact that the non-linear neuron algorithmically reaches larger capacities than the linear model, we observe that the algorithmic capacity of both algorithms is generally suboptimal with respect to the analytically calculated critical capacity, $\alpha_c(\theta_d, \theta_s)$ as shown in Fig. 5.

In the case of SGD, the difference between algorithmic capacity and analytical estimate is relatively mild at low θ_d , but the gap widens as the dendritic threshold increases. In the case of LAL, the discrepancy spans the entire range of θ_d , potentially due to the positive synaptic couplings inducing a hard optimization problem. The difference between algorithmic capacity and analytical RS estimate may be due to several factors, including RSB effects on the critical capacity (as the RS estimate represents an upper bound), finite K effects, and algorithmic hardness.

III. DISTRIBUTION OF SYNAPTIC WEIGHTS AND INPUT CONNECTIVITY SPARSITY

We next turned to the calculation of the distribution of synaptic weights in our neuron with non-linear dendritic integration. In a perceptron with sign-constrained weights, it has been shown that this distribution contains a delta function at zero ('silent' or 'potential' synapses), and a truncated Gaussian distribution of non-negative weights, at maximal capacity [32, 38],

$$P(W) = p_0 \delta(W) + \frac{1}{\sqrt{2\pi}W_*} e^{-\frac{(W+BW_*)^2}{2W_*^2}} \Theta(W) \quad (6)$$

where $\Theta(\cdot)$ is the Heaviside function. The fraction of silent weights is a simple function of B , $p_0 = H(-B) \equiv \frac{1}{2}\text{Erfc}\left(-\frac{B}{\sqrt{2}}\right)$, whereas B , W_* depend on parameters of the model. In the absence of robustness constraints, the fraction of silent synapses p_0 is exactly 50%, but this fraction increase in the presence of robustness constraints. Furthermore, it has been shown that such a distribution can fit well data from both cerebellar Purkinje cells [38, 52], and cortical pyramidal cells [31, 32], but only with a strong robustness constraints, consistent with

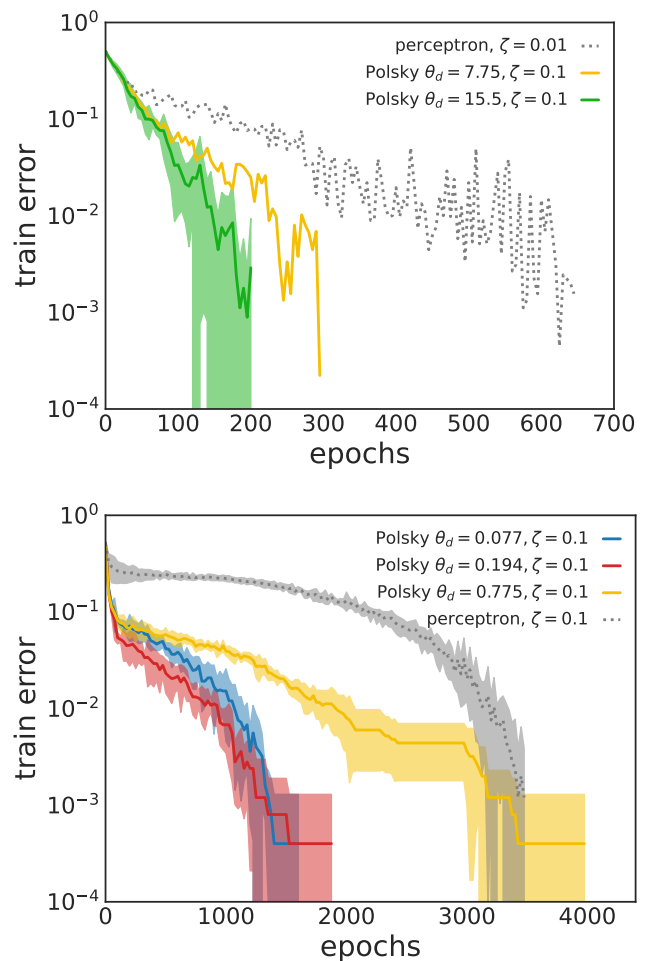


Figure 4. **Training speed.** Comparison of the convergence times of linear and non-linear neuron models using LAL (Algo. 2, upper panel) and SGD (Algo. 1, lower panel). The total fraction of patterns is fixed at $\alpha = 0.5$ for SGD and $\alpha = 0.9$ for LAL, ensuring that both algorithms can perfectly learn the training set with both the linear and non-linear neuron models. For both neuron models, the number of synapses (i.e., the input size) is $N = 999$, and the number of dendritic branches for the non-linear neuron is $K = 27$. Each curve is averaged over 10 realizations of the initial conditions.

idea that these networks optimize storage capacity with a strong robustness constraint, or vice versa optimize robustness of stored information. The obtained strong robustness derives from the experimentally observed low connection probabilities, ~ 0.2 in granule cell to Purkinje cell connections, and ~ 0.1 in layer 5 recurrent pyramidal cell connections.

It is worth mentioning that, from machine learning standpoint, finding solutions with large margin is desirable for many aspects, such as noise control of input perturbations, or to achieve a good test accuracy. In [48, 51] it has been shown that high-margin solutions possess a larger number of flat directions in the loss landscape; this

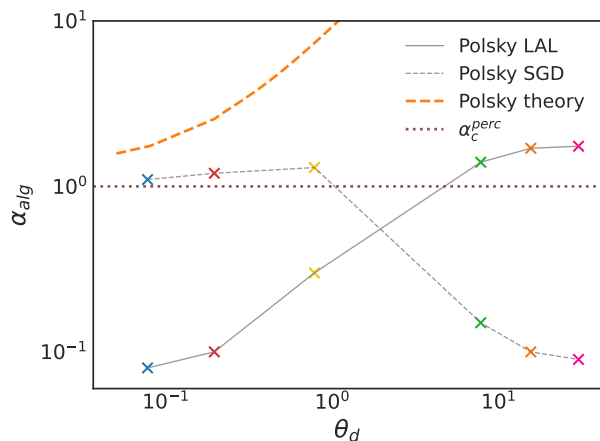


Figure 5. Algorithmic capacity for LAL (Algo. 2) and SGD (Algo. 1), compared to the analytical RS estimate in function of the dendritic threshold θ_d . Same parameters of Fig. 3. The critical capacity of the perceptron (dashed line) is $\alpha_c^{\text{perc}} = 1$.

means that one could potentially reduce the number of parameters without a significant performance drop, effectively making the network sparse. As we show in the next section, our two-layer neuron model is able to produce realistic and large connection sparsity by exploiting the dendritic non-linearity, without imposing any explicit robustness constraint.

Non-linearity automatically induces connection sparsity

To investigate the impact of the dendritic non-linearity on both the connectivity sparsity and the whole distribution of synaptic weights, we computed the $P(W)$ of models with dendritic non-linearities. As we show in the SI, in the large K limit, the functional form of the distribution of synaptic weights is exactly the same as the one obtained for the perceptron, for any value of α , and in particular in the critical capacity limit as in (6). However, the values of p_0 , B , W_\star depend *strongly* on the type of non-linearity used, even when the reliability parameter κ vanishes.

We show in Fig. 6 the fraction of silent synapses p_0 as a function of the dendritic threshold θ_d , for the experimentally measured Polsky and for the ReLU non-linearity at maximal capacity. We see that the experimentally measured non-linearity is capable of greatly increasing synaptic sparsity, in the absence of a robustness requirement during learning. In addition, because Polsky saturates at large preactivations, it is also able to maintain a large value of the sparsity even at large values of θ_d ; in this same regime the ReLU non-linearity tends to decrease the number of silent synapses and approaches the sparsity level present in the one-layer neuron model.

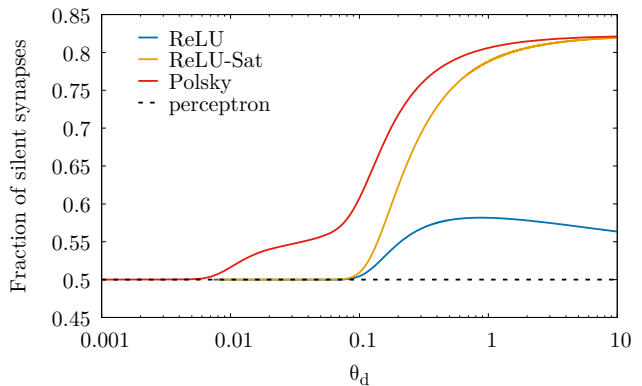


Figure 6. Fraction of silent synapses at maximal capacity as a function of the dendritic inhibition threshold for the Polsky ($x_{\min} = 0.33$ and $\gamma = 15$, red line), ReLU (blue) and ReLU-Sat (orange) non-linearities. Here we have fixed the input and output coding levels $f_{\text{in}} = f_{\text{out}} = 0.5$, the somatic threshold to $\theta_s = 0.5$ and the reliability parameter $\kappa = 0$. The dashed black line corresponds to the case of the linear neuron model, in which the fraction of silent synapses remains constant at 0.5, since $\kappa = 0$.

Comparison with experimental data

We next fitted the analytical distribution of synaptic weights of the non-linear neuron model to the experimental data of $P(W)$ recorded in [31] using quadruple patch intracellular recordings of rat cortical pyramidal cells. The observed connection probability in these recordings is ~ 0.12 . This connection probability is inaccessible to the non-linear model in the absence of robustness constraints. We chose instead $p_0 = 0.76$, which represents a good compromise between experimental recordings and biologically plausible parameters that allow us to reproduce p_0 with the variables of our model: $\{f_{\text{in/out}}, \theta_{d/s}, \sqrt{N/K}\}$. Once p_0 is fixed, we find W_\star (in mV) by fitting the experimental histogram of weights with the expression in (6). Choosing $f_{\text{in/out}} = 0.05$, we then obtain θ_d by using the saddle point relation

$$\theta_d = f_{\text{in}} W_\star [G(B) - BH(B)] \quad (7)$$

Finally, we can choose θ_s in order to obtain from the saddle point equations the value of $p_0 = 0.76$ that was chosen initially.

Fig. 7 shows that the resulting distribution agrees well with experimental data. We stress that contrary to the case of linear neuron model, our fitting procedure did not rely on the robustness parameter κ as a fitting parameter in order to induce sparsity in the model.

Synaptic weight distributions at algorithmic capacities Our numerical simulations, using both SGD and LAL, show that at algorithmic capacity, the distribution becomes well described by a delta function at zero, with

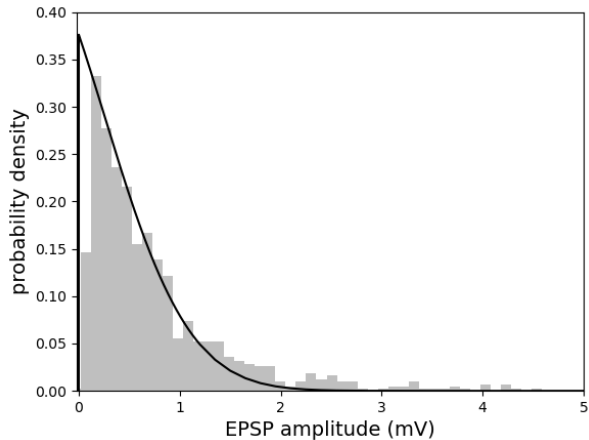


Figure 7. Experimental distribution of synaptic weights vs theoretical distribution at maximal capacity (see equation (6)) using as fitting parameters the dendritic and somatic inhibitory thresholds, respectively θ_d and θ_s . For $f_{in} = f_{out} = 0.05$ and $x_{min} = 0.2$, $\gamma = 20$ we have obtained in biological units, we find $\theta_d \simeq 0.6$ mV and $\theta_s \simeq 63$ mV.

a finite fraction of zero weights, and a truncated Gaussian describing positive weights. However, the fraction of zero weight synapses at algorithmic capacity is significantly below the analytically calculated one, and is close to 50%. This is not surprising, because, as mentioned above, the algorithmic capacity is below the analytical capacity based on a RS calculation.

IV. NOISE ROBUSTNESS AND GENERALIZATION

Robustness to input and synaptic noise

Noise is a ubiquitous feature at all levels of the nervous system, from the molecular to the whole brain level [54]. In particular, single neurons operate in a highly noisy environment, due to background inputs they constantly receive. Thus, robustness to input and synaptic noise are fundamental computational requirements for any realistic single neuron model. We thus turn to an investigation of robustness of our model to noise. In our simulations, we estimate the robustness to input noise by independently flipping the entries of each pattern in the training set with probability ρ maintaining the same label and measuring the train error of optimal synaptic configurations on this corrupted training set. The left column of Fig. 8 shows the robustness to input noise for LAL (top panel) and SGD (bottom panel). We observe that the non-linear model is more robust to input perturbations compared to the linear model with the same number of synaptic param-

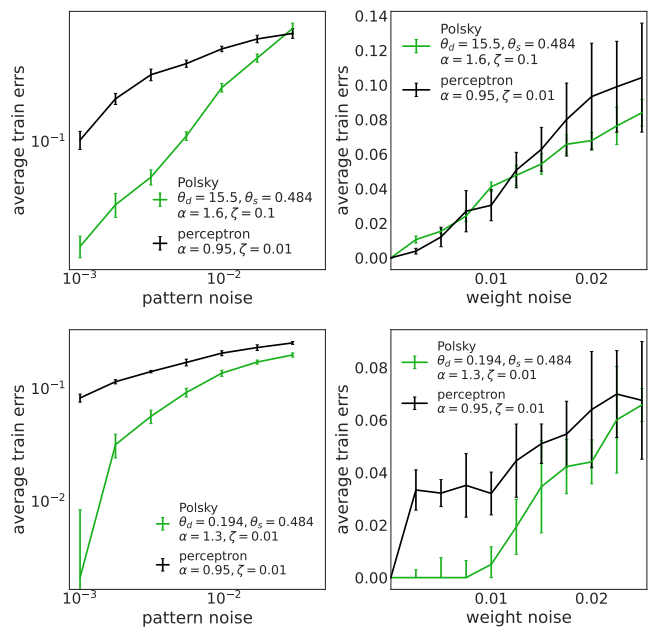


Figure 8. **Robustness to input and synaptic noise in the storage case.** Left column: Robustness to input noise, measured as the increase in the fraction of misclassified patterns as a function of input flipping probability (upper panel: LAL; lower panel: SGD). Right column: Robustness to synaptic noise, measured as the increase in the fraction of misclassified patterns as a function of the amplitude of Gaussian synaptic noise (upper panel: LAL; lower panel: SGD). Note that synaptic noise robustness is consistent with the *local energy* definition [53]. For both neuron models, the number of synapses (i.e., the input size) is $N = 999$, and the number of dendritic branches for the non-linear neuron is $K = 27$. Each curve represents the average over 10 realizations of the initial conditions.

ters. Similarly, we measure synaptic noise robustness by estimating the number of misclassified patterns when synaptic strengths are perturbed by applying a multiplicative Gaussian noise of amplitude σ to zero-error synaptic configurations \mathbf{W} . In practice, we measure the quantity $\delta E_{\text{train}}(\mathbf{W}, \sigma) = \mathbb{E}_{\mathbf{z}} E_{\text{train}}([\mathbf{W} + \sigma \mathbf{z} \odot \mathbf{W}]_+) - E_{\text{train}}(\mathbf{W})$, where $E_{\text{train}}(\mathbf{W})$ is the number of errors made by configuration \mathbf{W} on the training set, the expectation $\mathbb{E}_{\mathbf{z}}$ is over normally distributed synaptic noise realizations $\mathbf{z} \sim \mathcal{N}(0, I_N)$, \odot is the element-wise product, and $[\cdot]_+$ is the ReLU function. The quantity $\delta E_{\text{train}}(\mathbf{W}, \sigma)$ is also known as the *local energy* in the machine and deep learning literature. It serves as a proxy for the flatness of the energy landscape around a given optimal configuration [53, 55]. It is worth noting that a synaptic hard threshold at zero is implemented in this case as well, meaning that synaptic configurations cannot take negative values even under perturbations, i.e. $\mathbf{W} > 0$ and $\mathbf{W} + \sigma \mathbf{z} \odot \mathbf{W} > 0$. Fig. 8 (right column) presents the robustness to synaptic noise of the linear and non-linear neurons for both the LAL (upper panel)

and SGD (bottom panel) algorithms. The results demonstrate that the dendritic non-linearity enhances synaptic noise robustness, or equivalently, the local energy landscape around optimal synaptic configurations is flatter in the non-linear case.

Generalization performance on real-world datasets

To study the generalization properties of the neuron model defined in (2), we focus on binary classification learning tasks using the MNIST [40], Fashion-MNIST [41], and CIFAR-10 [42] datasets, which are standard benchmarks in machine learning. The generalization error, a fundamental machine learning observable, can only be estimated in the presence of a test set, which is absent in the storage case. To ensure that the generalization tasks remain reasonably difficult while still allowing for generalization, we divide the MNIST and Fashion-MNIST datasets into an odd/even binary classification task. For MNIST, we separate odd and even digits into two different classes. Similarly, for Fashion-MNIST, we separate the classes corresponding to even and odd labels into two groups. For the CIFAR-10 dataset, we choose two different classes in order to define a reasonably difficult generalization task, namely Bird and Ship. The Methods section provides details on the dataset binarization procedure and hyperparameter selection. As shown in Fig. 9, the non-linear neuron demonstrates better performance on all the aforementioned generalization tasks. We have also verified that in more challenging scenarios, such as learning odd/even classes in the CIFAR-10 dataset (separating the classes into two groups based on their even or odd labels), the generalization error is very close to random guessing (around 40%).

V. CONCLUSIONS AND FUTURE DIRECTIONS

In this paper, we have studied the effect of realistic dendritic non-linearities on the computational abilities of a single neuron model with sign constrained synaptic weights. We have shown that dendritic non-linear integration is beneficial for multiple reasons. Firstly, it enhances the overall expressivity of a single neuron, measured as the maximum number of input-output associations that it can correctly store. Secondly, the non-linearity generates input connectivity sparsity in the model, i.e. it leads to a large fraction of zero weight (silent or potential) synapses, in the absence of any explicit robustness constraint. This is in marked contrast with previously analyzed neuron models with passive dendritic integration, in which a large level of sparsity as recorded experimentally in cerebellar Purkinje and pyramidal cells could only be obtained with a high re-

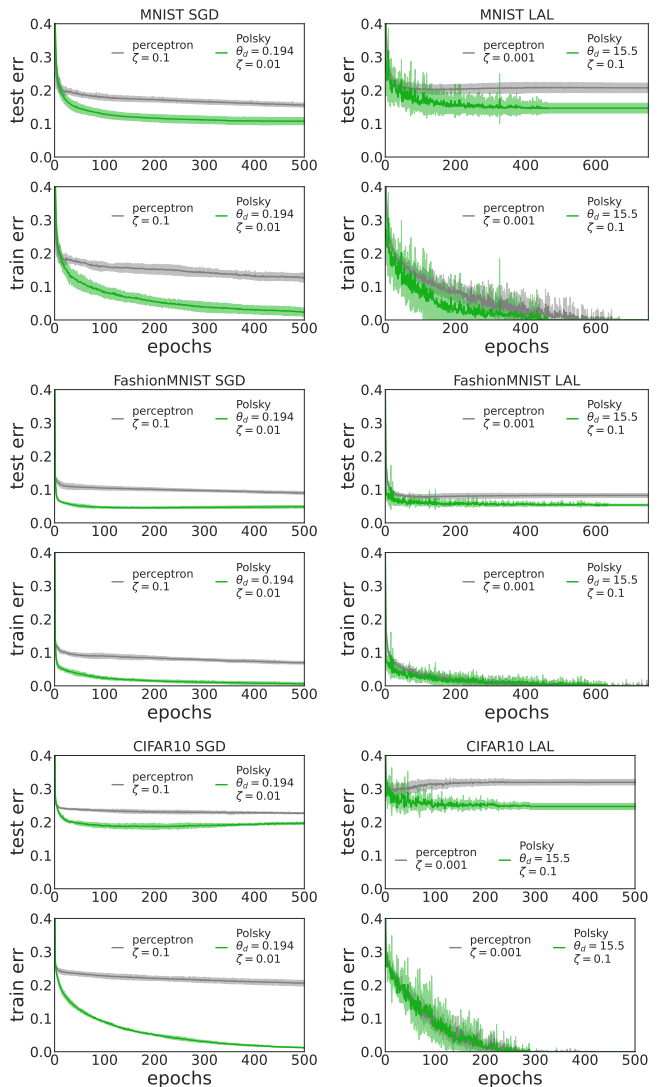


Figure 9. **Generalization capabilities on real-world datasets: MNIST, Fashion-MNIST, CIFAR-10.** Comparison of train and generalization errors of the non-linear neuron and the linear neuron using two learning algorithms: SGD (Algo.1, left column) and LAL (Algo.2, right column). Upper panels: MNIST (test and train error); Middle panels: Fashion-MNIST (test and train error); Lower panels: CIFAR-10 (test and train error). For both neuron models, the number of synapses (i.e., the input size) is $N = 1568$ for MNIST and Fashion-MNIST, and $N = 6144$ for CIFAR-10. The number of dendritic branches for the non-linear neuron is $K = 49$ for MNIST and Fashion-MNIST, and $K = 72$ for CIFAR-10. Each curve represents the average over 10 realizations of the initial conditions.

liability margin. In addition, the distribution of synaptic weights of our model shows a good agreement with the one recorded in experiments on pyramidal cells. On the algorithmic side, we quantified the benefit of nonlinear dendritic integration from several points of view. Firstly we have shown that nonlinear dendritic processing en-

ables algorithms such as SGD and LAL to find optimal synaptic configurations at larger density of input patterns with respect to linear integration, and to find them consistently faster. Secondly, we have found that synaptic configurations found by such algorithms have desirable computational properties in the non-linear case, such as a stronger robustness to input and synaptic noise, and higher generalization ability, compared to the linear case.

Algorithmically reaching the analytically calculated critical capacity α_c is challenging for both algorithms as shown in Fig. 5. Several factors contribute to the discrepancy between algorithmic and critical capacities. The critical capacity computed using RS serves as an upper bound for the true critical capacity, as RSB is likely to occur at lower values of α , a phenomenon well-established for both ReLU and step function non-linearities. Algorithmically, there is no guarantee to reach the optimal capacity, and finite-size effects from simulations with finite K and N could also influence results. Understanding this discrepancy will be the subject of future work.

Future work will concentrate on dropping some of the modelling assumptions we made here. For example, we have not considered the fact that there may be more than two layers of input processing through dendrites; this would make neurons more similar to deep tree networks. It would be therefore interesting to study the effect of multiple layers of dendritic integration on all the quantities studied in this paper. Similarly, it will be important to describe in a more realistic fashion inhibitory inputs, and the potential impact of inhibitory plasticity. Finally one should also take into account the effects of potential correlations structures in inputs, e.g. that inputs coming in the same branch are more correlated than inputs pertaining to different branches [56]. Similarly, synaptic inputs coming at different regions of the dendritic tree (e.g. basal vs apical) may have different statistical properties and convey different types of inputs.

Another important future direction concerns synaptic plasticity algorithms. Here, we have investigated simple plasticity algorithms (SGD and LAL) in a standard supervised learning scenario, in which a teaching signal is available to the neuron. In cerebellar Purkinje cells, this teaching signal could be implemented by the climbing fiber input, which has been shown to correlate with error in motor tasks. In cortical pyramidal cells, the presence of error signals is more speculative. In the presence of the error signal, SGD in a single neuron model leads to a local plasticity rule, that could be plausibly implemented in a biological neuron, unlike in multi-layer networks (see Methods). Finally, it will be interesting to investigate the computational abilities of a neuron with non-linear dendrites in a purely unsupervised learning setting.

Analytical Methods

The entropy in (5) can be computed using the replica method; since the average over the log in (5) is difficult to compute one uses the identity $\ln(x) = \lim_{n \rightarrow 0} \frac{x^n - 1}{n}$. Taking n as a positive integer one ends to deal with an enlarged system of n identical virtual copies of the system, so that the average can be easily be performed, at the price to couple the replicas together. However in the large N limit, it turns out that the properties of the model can be fully characterized by a finite set of quantities called order parameters that are determined self-consistently by solving equations obtained by saddle point method (see also the recent notes [44] for a more pedagogical introduction). In practice, the averaged entropy can be fully characterized by the order parameters

$$\sum_{i=1}^{N/K} W_{li}^a = \frac{N}{K} \bar{W} + \sqrt{\frac{N}{K}} M_l^a \quad (8a)$$

$$q_l^{ab} \equiv \frac{K}{N} \sum_{i=1}^N W_{li}^a W_{li}^b \quad (8b)$$

$$Q_l^a \equiv \frac{K}{N} \sum_{i=1}^N (W_{li}^a)^2 \quad (8c)$$

and their conjugated ones \hat{M}_l^a , \hat{q}_l^{ab} , \hat{Q}_l^a , with $a, b \in [n]$ and $l \in [K]$. They represent respectively: the typical average synaptic weight, the most probable overlap between two replicas extracted from the Gibbs measure in (4), and the typical averaged squared norm of a synaptic weights belonging to the dendritic branch $l \in [K]$. Since the fields are non-overlapping, each branch has access only to a portion of the synaptic input; therefore there is no correlation between hidden units in the same architecture. Notice also that, in (A11a), the average can be expressed with the sum of two contributions: the first represents the average of the scaled synaptic weights $\bar{W} = \frac{\theta_d}{f_{in}}$, while the second represents a $\sqrt{\frac{N}{K}}$ correction needed to fine tune this average with respect to the threshold θ_d . We report in the SI the full analytical calculations of the entropy (5) in the case in which the structure of the overlap matrix q_l^{ab} is symmetric under permutation over the replica indices (the so called ‘‘Replica Symmetric’’ or RS ansatz), and the order parameters do not depend on replica and dendritic branch indices $l \in [K]$. This means $q_l^{ab} = Q\delta_{ab} + q(1 - \delta_{ab})$, $\forall a, b \in [n]$ and $l \in [K]$ and similarly for the other order parameters. The entropy can be therefore obtained by maximizing a function ϕ_{RS} with respect to the order parameters

$$\phi = \max_{q, \hat{q}, Q, \hat{Q}, M, \hat{M}} \phi_{RS}(q, \hat{q}, Q, \hat{Q}, M, \hat{M})$$

ϕ_{RS} can be written as

$$\phi_{RS} = \mathcal{G}_S + \alpha \mathcal{G}_E. \quad (9)$$

i.e. as a sum of an entropic contribution \mathcal{G}_S which represent the log of the total volume of configurations \mathbf{W} , and an energetic part \mathcal{G}_E that corresponds to the log of the fraction of solutions for a given α . The explicit expressions of \mathcal{G}_S and \mathcal{G}_E are reported in the SI.

The values of the order parameters $q, \hat{q}, Q, \hat{Q}, M, \hat{M}$ can be found by solving a set of coupled saddle point equations obtained by equating to zero the derivative of ϕ_{RS} with respect to each of them.

Limit of large number of dendritic branches

As noted in [33–35], pyramidal cells receive roughly 10000 synaptic inputs, which are dispersed across a wide range of dendritic branches, varying from several dozen to several hundred. This motivates considering the limits where N and K tend towards infinity, but with the K/N approaching zero.

On the technical side, solving the saddle point equations for generic K is in general a very difficult task, since in order to compute the energetic term one should evaluate $2K$ -dimensional integrals. However in the large K limit the energetic term simplifies considerably. Indeed, because of the Central Limit Theorem, for K large the total inputs to the soma are Gaussian distributed variables with mean and variance that depend on the transfer function implemented by dendrites.

Interestingly, as first observed in [24], the final expression which we derive in detail in the SI, becomes equal to an *effective perceptron*, i.e. the entropy is in form equal to the one presented in [32, 38] for the one-layer neuron model, but where each order parameter is substituted by an integral expression that depends on the activation function g used.

Biological parameters

In order to estimate biologically plausible parameters for the non-linear neuron model and the Polsky transfer function, we refer to Fig. 4c of [13], for a pair of EPSPs and a single EPSP. In particular, with the saturation of the Polsky transfer function in $x = 1, y = 1$ on both the x -axis and the y -axis, we obtain that the biologically realistic ranges for the Polsky parameters are (in units of $15 mV$): $x_{\min} \in [0.2, 0.33]$, $\gamma \in [13, 20]$.

Here below we also report the conversion factors that we have used to convert the quantities of the model to biological ones. Let's call W_b the biological measurement of a weight (in mV) and the corresponding one of the model W . They are related by

$$W_b = \frac{15W}{\sqrt{N}}. \quad (10)$$

The dendritic threshold of the model defined in (2a) is related to the biological one by

$$\theta_{db} = \frac{15}{\sqrt{N}} \frac{N}{K} \theta_d = \frac{15\sqrt{N}}{K} \theta_d \quad (11)$$

For the fitting procedure of the theoretical distribution (6) on the experimental distribution of synaptic weights, we got $W_* \simeq 5.56 mV$, using $p_0 = 0.76$. This corresponds, applying the conversions above, to a dendritic threshold of $\theta_d \simeq 0.6 mV$, having chosen $\sqrt{N} \simeq K$ and $\sqrt{N} = 100$. The somatic conversion factor is instead

$$\theta_{sb} = K\theta_s. \quad (12)$$

Learning algorithms

Inspired by machine learning practice, we use a modified version of the Stochastic Gradient Descent (SGD) algorithm, capable of dealing with strictly positive weights, to train our single neuron models (see Algo. 1). To constrain the synapses to be positive during the learning dynamics, at each gradient step, we reset negative synaptic weights to zero. The SGD algorithm minimizes a differentiable objective function, and a common choice in machine learning is the cross-entropy (CE) loss. For binary outputs, the CE loss is given by: $\mathcal{L}_{CE}(\mathbf{W}; \gamma_{ce}, \theta_d, \theta_s) = \sum_{\mu=1}^P f_{\gamma_{ce}}(\sigma^\mu \Delta^\mu(\mathbf{W}; \theta_d, \theta_s))$ where $f_{\gamma_{ce}}(x) = -\frac{x}{2} + \frac{1}{2\gamma_{ce}} \log(2 \cosh(\gamma_{ce}x))$ and the output pre-activation is given by $\Delta^\mu(\mathbf{W}; \theta_d, \theta_s) = \frac{1}{\sqrt{N}} \sum_{i=1}^N W_i \xi_i - T\sqrt{N}$ for the linear neuron and (2b) for the nonlinear neuron. The parameter γ_{ce} governs the shape of the CE loss function and, consequently, the training robustness, as discussed in [27].

Note that unlike in multi-layer networks, SGD in a single neuron model leads to a local learning rule, that could be plausibly implemented in a biological neuron, provided an error signal is available. For a single presented pattern μ , a weight w_{il} is changed by an amount proportional to $\delta w_{il} = -\sigma^\mu f'_{\gamma_{ce}}(\sigma^\mu \Delta^\mu) g'(\lambda_l^\mu) \xi_{il}^\mu$. This can be interpreted as a ‘three factor rule’, where $-\sigma^\mu f'_{\gamma_{ce}}$ is a ‘soft’ error signal available to the whole neuron (possibly a ‘plateau potential’ triggered by apical inputs), $g'(\lambda_l^\mu)$ is a local, NMDA mediated, dendritic signal, and ξ_{il}^μ is the presynaptic activity.

Algorithm 1 SGD with CE loss and positive weights

Hyperparameters: learning rate ζ , cross-entropy parameter γ_{ce}

```

for  $t = 1, 2, \dots$  do
   $\xi^\mu, \sigma^\mu \leftarrow$  sample pattern
   $\delta w_{il} \leftarrow \nabla_{w_{il}} \mathcal{L}_{CE}(w_{il}; \xi^\mu, \gamma_{ce})$ 
   $w_{il} \leftarrow w_{il} - \zeta \cdot \delta w_{il}$ 
  if  $w_{il} < 0$  then
     $w_{il} \leftarrow 0$ 
  end if
end for
```

In Algo. 2, we define another algorithm capable of learning random binary $\{0, 1\}$ patterns on a non-linear neuron (tree committee machine) with positive synapses. This algorithm consists of modifications to the Least-Action Learning (LAL) algorithm [22, 27]. In practice, for each misclassified input pattern μ , we identify the dendritic branches that contribute most to the error by calculating the local stabilities $\delta_l^\mu = \{\eta^\mu \lambda_l^\mu \text{ for } l \in \{1, \dots, K\}\}$, where $\eta^\mu = 2\sigma^\mu - 1$ and λ_l^μ is defined in (2c), and selecting the branches for which $\delta_l^\mu < 0$. Using the perceptron rule, we update a subset l_\star of branches corresponding to a certain fraction p of the ones contributing to the error (we set $p = 0.5$). Alternatively, it is possible to update the easiest dendritic branch to fix, i.e. $l_\star = \operatorname{argmax}(\delta_l^\mu : \delta_l^\mu < 0)$, which corresponds to the original LAL rule, with comparable performances. Synapses are reset to zero whenever they become negative, and the algorithm automatically stops when a zero-error synaptic configuration is found.

Algorithm 2 LAL with positive weights

Hyperparameters: learning rate ζ
for $t = 1, 2, \dots$ **do**
 $\xi^\mu, \sigma^\mu \leftarrow$ sample pattern
 Calculate neuronal output $\hat{\sigma}$ as per (2a)
 if $\hat{\sigma} \neq \sigma^\mu$ **then**
 $\eta^\mu = 2\sigma^\mu - 1$
 $\delta_l^\mu = \{\eta^\mu \lambda_l^\mu \text{ for } l \in \{1, \dots, K\}\}$ (see (2c))
 $l_\star = \{l^\mu : \delta_l^\mu < 0 \text{ with prob. } p\}$ \triangleright Select a random
 fraction $p = 0.5$ of branches that contribute to the error
 $w_{il_\star} \leftarrow w_{il_\star} + \zeta \cdot \eta^\mu \cdot \xi_{il_\star}^\mu$
 if $w_i < 0$ **then**
 $w_i \leftarrow 0$
 end if
 end if
end for

Numerical Experiments

We provide details and algorithmic considerations used for the numerical experiments reported in the paper for both the linear and non-linear neuron models.

For the non-linear neuron model, the hyper-parameters are the two thresholds θ_d and θ_s , the learning rate ζ , and the CE robustness parameter γ_{ce} (for the SGD algorithm). For the linear neuron model, there are only two parameters: the learning rate ζ and the robustness parameter γ_{ce} (for SGD). In the linear case, the threshold θ_d governs the synaptic mean value but does not alter the dynamics with a suitable rescaling of the learning rate with θ_d . We choose the non-linear neuron’s thresholds θ_d and θ_s such that the input/output coding level mapping is maintained on average at initialization for numerical convenience (see SI for details). In the SGD case, the thresholds must also consider the fact that the hidden layer pre-activations have to be distributed in the active

range of the g_{polsky} transfer function for the algorithm to work. We perform an exponential annealing of the learning rate: at epoch t , the learning rate is $\zeta t = \zeta(1 - d\zeta)^t$ with $d\zeta = 10^{-4}$. Learning rate decay is justified by the fact that in the linear neuron case, adapting [1, 57] convergence proof, one can demonstrate that the perceptron algorithm converges below the critical capacity, provided that the variation in weights at each step is smaller than a certain critical value $dw_c > 0$ [38]. During single-neuron training, we present one input pattern at a time (the *minibatch size* is 1). We randomly shuffle the pattern sequence at each dataset presentation (*epoch*). Input and output coding levels are fixed to $f_{\text{in}} = f_{\text{out}} = 0.5$. See the SI for further discussion on how to choose hyper-parameters.

Synapses are initialized uniformly at random between zero and twice the theoretical expected value of the mean weight $\bar{w} = \frac{\theta}{f_{\text{in}}N}$. This is the expected value for both the linear and non-linear neurons with a generic activation function and a generic value of the θ_s threshold in the symmetric $f_{\text{in}} = f_{\text{out}} = 0.5$ case, as analytically shown in the SI. If synapses turn negative during training, a hard boundary condition is enforced, and they are immediately reset to zero. For the non-linear neuron, the SGD update rule (Algo.1) with the cross-entropy loss and the LAL update rule (Algo.2) are performed only on the dendritic branches of the first synaptic layer.

For the linear neuron trained with the SGD algorithm, the dynamics is invariant with respect to the rescaling by a positive constant c of the three hyper-parameters: ζ , γ_{ce} , and θ_d , i.e.: $\zeta \leftarrow \zeta/c$, $\gamma_{ce} \leftarrow c\gamma_{ce}$, $\theta_d \leftarrow \theta_d/c$. As a result, the dynamics effectively depends only on two of these hyper-parameters. The same consideration holds for the LAL algorithm but with only the two hyper-parameters ζ and θ_d , such that the dynamics effectively depends only on one of them.

Real datasets definition and binarization

It is necessary to define a binarization procedure for real-world classification datasets (MNIST, FashionMNIST, CIFAR10) such that different classes have comparable input coding levels. Otherwise, as can be observed even in a simple teacher-student setting, the classification task becomes trivial due to the inherent correlation between neuronal classification and coding level, arising from the strictly positive nature of both input patterns and synapses.

One possible choice is to binarize the patterns of real-world datasets into zeros and ones, with a binarization threshold determined by the median value of each pattern. However, there still is an ambiguity in this approach: we can assign zero to pixels below the median and one to pixels above it, or vice versa. These two choices may potentially result in different input pattern

coding levels when patterns are imbalanced. To address both this binarization ambiguity and trivial correlations between neuronal classification and coding level, a possible approach is to integrate both binarization types within the same pattern. Consequently, both the input size and the number of synaptic weights for each neuron double. Instances of neurons being active in the absence of input have been observed, for example, in [58]. To further reduce intra-branch correlations, pixels in each image are shuffled using the same random permutation prior to binarization. Moreover, to maintain the input locality to the dendritic branch, each branch receives a different, non-overlapping portion of the pattern that combines both binarization choices. In the case of Fashion-MNIST, we filter the patterns that have strictly positive median to avoid extremely unbalanced input coding level cases. However, such cases are unavoidable in the MNIST dataset due to the black-digit-on-white-background nature of the dataset.

Hyper-parameter selection

We report the hyper-parameter selection used for numerical simulations of the non-linear neuron (a.k.a. tree committee machine) and the linear one (a.k.a. perceptron). In the storage case, the input size is $N = 999$, and the number of dendritic branches of the non-linear neuron is $K = 27$. For numerical simulations on real-world datasets, the input size is twice the number of pixels in each image, i.e., $N = 1568$ for MNIST and FashionMNIST, and $N = 6144$ for CIFAR10. The number of dendritic branches is $K = 7$ for MNIST and FashionMNIST, and $K = 8$ for CIFAR10. The Polsky dendritic nonlinear transfer function has biologically estimated parameters $x_{\min} = 0.22$ and $\gamma = 18$. The non-linear neuron behavior regarding relevant observables is studied as a function of the dendritic and somatic thresholds θ_d and θ_s .

To optimize neuronal computational performances on relevant observables, we perform a grid search for SGD on the learning rate $\zeta \in \{0.0001, 0.001, 0.01, 0.1, 1.0\}$ and the cross-entropy robustness parameter $\gamma_{ce} \in \{0.001, 0.01, 0.1, 1.0, 10.0, 100.0\}$. For LAL, we search the learning rate in $\zeta \in \{0.0001, 0.001, 0.01, 0.1, 1.0\}$. For both algorithms, the learning rate decay $d\zeta$ is fixed to 10^{-4} .

ACKNOWLEDGEMENTS

This paper is dedicated to the memory of our colleague and friend Luca Trevisan. F.P. acknowledges support by the PNRR-PE-AI FAIR project funded by the NextGeneration EU program. E.M.M. acknowledges the MUR-Prin 2022 funding Prot. 20229T9EAT, financed by the European Union (Next Generation EU).

- [1] M. Minsky and S. A. Papert, *Perceptrons - Expanded Edition* (MIT Press, 1988).
- [2] T. M. Cover, Geometrical and statistical properties of systems of linear inequalities with applications in pattern recognition., *IEEE Trans EC-14*, 326 (1965).
- [3] E. Gardner, The space of interactions in neural network models, *Journal of Physics A: Mathematical and General* **21**, 257 (1988).
- [4] A. Engel and C. Van den Broeck, *Statistical mechanics of learning* (Cambridge University Press, 2001).
- [5] M. London and M. Häusser, Dendritic computation, *Annual Review of Neuroscience* **28**, 503 (2005), PMID: 16033324, <https://doi.org/10.1146/annurev.neuro.28.061604.135703>.
- [6] M. Larkum, A cellular mechanism for cortical associations: an organizing principle for the cerebral cortex, *Trends Neurosci.* **36**, 141 (2013).
- [7] G. Major, M. E. Larkum, and J. Schiller, Active properties of neocortical pyramidal neuron dendrites, *Annu. Rev. Neurosci.* **36**, 1 (2013).
- [8] J. Schiller, G. Major, H. J. Koester, and Y. Schiller, NMDA spikes in basal dendrites of cortical pyramidal neurons, *Nature* **404**, 285 (2000).
- [9] T. Branco and M. Häusser, Synaptic integration gradients in single cortical pyramidal cell dendrites, *Neuron* **69**, 885 (2011).
- [10] M. E. Larkum, J. J. Zhu, and B. Sakmann, A new cellular mechanism for coupling inputs arriving at different cortical layers, *Nature* **398**, 338 (1999).
- [11] M. E. Larkum, W. Senn, and H.-R. Luscher, Top-down dendritic input increases the gain of layer 5 pyramidal neurons, *Cereb Cortex* **14**, 1059 (2004).
- [12] T. Nevian, M. E. Larkum, A. Polsky, and J. Schiller, Properties of basal dendrites of layer 5 pyramidal neurons: a direct patch-clamp recording study, *Nat Neurosci* **10**, 206 (2007).
- [13] A. Polsky, B. W. Mel, and J. Schiller, Computational subunits in thin dendrites of pyramidal cells, *Nature neuroscience* **7**, 621 (2004).
- [14] P. Poirazi, T. Brannon, and B. W. Mel, Pyramidal neuron as two-layer neural network, *Neuron* **37**, 989 (2003).
- [15] N. Brunel, V. Hakim, and M. J. Richardson, Single neuron dynamics and computation, *Current Opinion in Neurobiology* **25**, 149 (2014), theoretical and computational neuroscience.
- [16] B. B. Ujfalussy, J. K. Makara, M. Lengyel, and T. Branco, Global and Multiplexed Dendritic Computations under In-Vivo-like Conditions, *Neuron* **100**, 579 (2018).
- [17] M. E. Larkum, T. Nevian, M. Sandler, A. Polsky, and J. Schiller, Synaptic integration in tuft dendrites of layer 5 pyramidal neurons: A new unifying principle, *Science* **325**, 756 (2009), <https://www.science.org/doi/pdf/10.1126/science.1171958>.
- [18] D. Beniaguev, I. Segev, and M. London, Single cortical neurons as deep artificial neural networks, *Neuron* **109**, 2727 (2021).
- [19] M. Pagkalos, R. Makarov, and P. Poirazi, Leveraging dendritic properties to advance machine learning and neuro-inspired computing, *Current Opinion in Neurobiology* **85**, 102853 (2024).

- [20] S. Sardi, R. Vardi, A. Sheinin, A. Goldental, and I. Kanter, New types of experiments reveal that a neuron functions as multiple independent threshold units, *Scientific reports* **7**, 18036 (2017).
- [21] G. J. Mitchison and R. M. Durbin, Bounds on the learning capacity of some multi-layer networks, *Biol. Cybern.* **60**, 345–365 (1989).
- [22] E. Barkai, D. Hansel, and H. Sompolinsky, Broken symmetries in multilayered perceptrons, *Phys. Rev. A* **45**, 4146 (1992).
- [23] R. Monasson and R. Zecchina, Weight space structure and internal representations: A direct approach to learning and generalization in multilayer neural networks, *Physical Review Letters* **75**, 2432–2435 (1995).
- [24] C. Baldassi, E. M. Malatesta, and R. Zecchina, Properties of the geometry of solutions and capacity of multilayer neural networks with rectified linear unit activations, *Physical Review Letters* **123**, 10.1103/physrevlett.123.170602 (2019).
- [25] J. A. Zavatone-Veth and C. Pehlevan, Activation function dependence of the storage capacity of treelike neural networks, *Phys. Rev. E* **103**, L020301 (2021).
- [26] C. Baldassi, C. Borgs, J. T. Chayes, A. Ingrosso, C. Lucibello, L. Saglietti, and R. Zecchina, Unreasonable effectiveness of learning neural networks: From accessible states and robust ensembles to basic algorithmic schemes, *Proceedings of the National Academy of Sciences* **113**, E7655 (2016), <https://www.pnas.org/content/113/48/E7655.full.pdf>.
- [27] C. Baldassi, F. Pittorino, and R. Zecchina, Shaping the learning landscape in neural networks around wide flat minima, *Proceedings of the National Academy of Sciences* **117**, 161 (2020), <https://www.pnas.org/content/117/1/161.full.pdf>.
- [28] C. Lucibello, F. Pittorino, G. Perugini, and R. Zecchina, Deep learning via message passing algorithms based on belief propagation, *Machine Learning: Science and Technology* **3**, 035005 (2022).
- [29] B. L. Annesi, C. Lauditi, C. Lucibello, E. M. Malatesta, G. Perugini, F. Pittorino, and L. Saglietti, Star-shaped space of solutions of the spherical negative perceptron, *Phys. Rev. Lett.* **131**, 227301 (2023).
- [30] K. Hornik, Approximation capabilities of multilayer feed-forward networks, *Neural Networks* **4**, 251 (1991).
- [31] S. Song, P. J. Sjöström, M. Reigl, S. Nelson, and D. B. Chklovskii, Highly nonrandom features of synaptic connectivity in local cortical circuits, *PLoS biology* **3**, e68 (2005).
- [32] N. Brunel, Is cortical connectivity optimized for storing information?, *Nature neuroscience* **19** (2016).
- [33] V. Braitenberg and A. Schütz, *Anatomy of the cortex* (Springer-Verlag, 1991).
- [34] D. M. Iascone, Y. Li, U. I. M. Doron, H. Chen, V. Andreu, F. Goudy, H. Blockus, L. F. Abbott, I. Segev, H. Peng, and F. Polleux, Whole-Neuron Synaptic Mapping Reveals Spatially Precise Excitatory/Inhibitory Balance Limiting Dendritic and Somatic Spiking, *Neuron* **106**, 566 (2020).
- [35] G. N. Elston, R. Benavides-Piccione, A. Elston, P. R. Manger, and J. Defelipe, Pyramidal cells in prefrontal cortex of primates: marked differences in neuronal structure among species, *Front Neuroanat* **5**, 2 (2011).
- [36] E. Gardner and B. Derrida, Optimal storage properties of neural network models, *Journal of Physics A: Mathematical and General* **21**, 271 (1988).
- [37] D. Amit, K. Y. Wong, and C. Campbell, Perceptron learning with sign-constrained weights, *Journal of Physics A* **22**, 2039 (1989).
- [38] N. Brunel, V. Hakim, P. Isope, J.-P. Nadal, and B. Barbour, Optimal information storage and the distribution of synaptic weights: Perceptron versus purkinje cell, *Neuron* **43**, 745 (2004).
- [39] M. Stojnic, Capacity of the treelike sign perceptrons neural networks with one hidden layer—rdt based upper bounds, arXiv preprint arXiv:2312.08244 (2023).
- [40] Y. LeCun, C. Cortes, C. Burges, *et al.*, Mnist handwritten digit database (2010).
- [41] H. Xiao, K. Rasul, and R. Vollgraf, Fashion-mnist: a novel image dataset for benchmarking machine learning algorithms (2017), [cs.LG/1708.07747](https://arxiv.org/abs/1708.07747).
- [42] V. N. Alex Krizhevsky and G. Hinton, Cifar-10 (canadian institute for advanced research), - (2009).
- [43] C. Clopath, J.-P. Nadal, and N. Brunel, Storage of correlated patterns in standard and bistable purkinje cell models, *PLOS Computational Biology* **8**, 1 (2012).
- [44] E. M. Malatesta, High-dimensional manifold of solutions in neural networks: insights from statistical physics, arXiv preprint arXiv:2309.09240 (2023).
- [45] M. Mezard, G. Parisi, and M. Virasoro, *Spin glass theory and beyond: An Introduction to the Replica Method and Its Applications*, Vol. 9 (World Scientific Publishing Company, 1987).
- [46] G. Parisi, Infinite number of order parameters for spin-glasses, *Phys. Rev. Lett.* **43**, 1754 (1979).
- [47] A. Engel, H. M. Köhler, F. Tschepke, H. Vollmayr, and A. Zippelius, Storage capacity and learning algorithms for two-layer neural networks, *Phys. Rev. A* **45**, 7590 (1992).
- [48] C. Baldassi, E. M. Malatesta, G. Perugini, and R. Zecchina, Typical and atypical solutions in nonconvex neural networks with discrete and continuous weights, *Phys. Rev. E* **108**, 024310 (2023).
- [49] B. L. Annesi, E. M. Malatesta, and F. Zamponi, In preparation (2024).
- [50] C. Baldassi, A. Ingrosso, C. Lucibello, L. Saglietti, and R. Zecchina, Subdominant dense clusters allow for simple learning and high computational performance in neural networks with discrete synapses, *Phys. Rev. Lett.* **115**, 128101 (2015).
- [51] C. Baldassi, C. Lauditi, E. M. Malatesta, G. Perugini, and R. Zecchina, Unveiling the structure of wide flat minima in neural networks, *Phys. Rev. Lett.* **127**, 278301 (2021).
- [52] P. Isope and B. Barbour, Properties of unitary granule cell: Purkinje cell synapses in adult rat cerebellar slices, *Journal of Neuroscience* **22**, 9668 (2002).
- [53] F. Pittorino, C. Lucibello, C. Feinauer, G. Perugini, C. Baldassi, E. Demyanenko, and R. Zecchina, Entropic gradient descent algorithms and wide flat minima, in *International Conference on Learning Representations* (2021).
- [54] A. A. Faisal, L. P. Selen, and D. M. Wolpert, Noise in the nervous system, *Nat Rev Neurosci* **9**, 292 (2008).
- [55] F. Pittorino, A. Ferraro, G. Perugini, C. Feinauer, C. Baldassi, and R. Zecchina, Deep networks on toroids: Removing symmetries reveals the structure of flat regions in the landscape geometry, in *Proceedings of the 39th International Conference on Machine Learning*, Proceed-

- ings of Machine Learning Research, Vol. 162, edited by K. Chaudhuri, S. Jegelka, L. Song, C. Szepesvari, G. Niu, and S. Sabato (PMLR, 2022) pp. 17759–17781.
- [56] J. H. Kirchner and J. Gjorgjieva, Emergence of synaptic organization and computation in dendrites, *Neuroforum* **28**, 21 (2022).
- [57] F. Rosenblatt, *Principles of Neurodynamics* (Spartan Books, 1962).
- [58] K. Merten and A. Nieder, Active encoding of decisions about stimulus absence in primate prefrontal cortex neurons, *Proceedings of the National Academy of Sciences* **109**, 6289 (2012), <https://www.pnas.org/doi/pdf/10.1073/pnas.1121084109>.
- [59] E. Gardner, The space of interactions in neural network models, *Journal of Physics A: Mathematical and General* **21**, 257 (1988).

Impact of dendritic non-linearities on the computational capabilities of neurons

SUPPLEMENTAL INFORMATION

Clarissa Lauditi,¹ Enrico M. Malatesta,² Fabrizio Pittorino,^{2,3}
 Carlo Baldassi,² Nicolas Brunel,^{2,4} and Riccardo Zecchina²

¹*Department of Applied Math, John A. Paulson School of Engineering and Applied Sciences,
 Harvard University, 02138 Cambridge, MA, USA*

²*Department of Computing Sciences and Bocconi Institute for Data
 Science and Analytics (BIDSA), Bocconi University, 20136 Milano, Italy*

³*Department of Electronics, Information and Bioengineering, Politecnico di Milano, 20133 Milano, Italy*

⁴*Departments of Neurobiology and Physics, Duke University,
 Durham, North Carolina, United States of America*

CONTENTS

I. Single neuron model	2
Constraints on weights, excitation and inhibition	2
Dendritic non-linearity	2
Scaling of inputs and thresholds	3
Learning tasks	3
Learning algorithms	3
II. Storage capacity	3
Analytical methods	3
Critical capacity	4
Algorithmic capacity and learning speed	6
III. Distribution of synaptic weights and input connectivity sparsity	7
Non-linearity automatically induces connection sparsity	8
Comparison with experimental data	8
IV. Noise robustness and generalization	9
Robustness to input and synaptic noise	9
Generalization performance on real-world datasets	10
V. Conclusions and future directions	10
Analytical Methods	11
Limit of large number of dendritic branches	12
Biological parameters	12
Learning algorithms	12
Numerical Experiments	13
Real datasets definition and binarization	13
Hyper-parameter selection	14
Acknowledgements	14
References	14
A. Analytical results	18
1. Definition of the non-linear model of the neuron	18
2. Training set and partition function	18
3. Replica method	19
4. Replica Symmetric analysis	20
a. Large K limit	21

b. Free entropy and saddle point equations	23
c. Effective order parameters for some non-linearities	24
d. Small data regime	25
e. Distribution of dendritic preactivations	25
f. Limit of large somatic thresholds	26
5. Critical capacity	26
a. Limit of large dendritic threshold	28
b. Limit of small dendritic threshold	29
6. Distribution of synaptic weights	29
a. Distribution of synaptic weights in the maximal storage limit	30
B. Numerical experiments	30
1. Choice of the thresholds	30
2. Choice and scaling of the hyper-parameters	33

Appendix A: Analytical results

1. Definition of the non-linear model of the neuron

We recall here the main definitions of the single neuron model studied in the main text of the paper. Given an activity pattern $\xi^\mu \in \{0, 1\}^N$, the output of our model of neuron is obtained in two steps. Firstly, the activity pattern is processed by the corresponding dendritic branch; we suppose here that we have $l = 1, \dots, N/K$ dendritic branches each having a set of $i = 1, \dots, N$ positive synaptic weights W_{li} . The output activity τ_l^μ of a given branch l that corresponds to the activity pattern ξ^μ is obtained as

$$\tau_l^\mu = g \left(\sqrt{\frac{K}{N}} \sum_{i=1}^{N/K} W_{li} \xi_{li}^\mu - \sqrt{\frac{N}{K}} \theta_d \right) \equiv g(\lambda^\mu) \quad (\text{A1})$$

where θ_d is a threshold modeling inhibition at the level of the dendritic branch, while $g(\cdot)$ is a generic positive, (possibly) non-linear function. Secondly, the output of each branch is combined linearly by using another set of K synaptic weights c_l , $l = 1, \dots, K$ and the output is obtained as

$$\sigma_{\text{out}}^\mu = \Theta \left[\frac{1}{\sqrt{K}} \sum_{l=1}^K c_l \tau_l^\mu - \sqrt{K} \theta_s \right] \quad (\text{A2})$$

where $\Theta(x)$ is the Heaviside theta function that is 1 if $x > 0$ and 0 otherwise. The parameter θ_s is a threshold modelling inhibition coming from inhibitory neurons. In the following we will consider, for simplicity $c_l = 1$ for every $l = 1, \dots, K$.

2. Training set and partition function

We consider a training set composed of $P = \alpha N$ random i.i.d. activity patterns $\xi^\mu \in \{0, 1\}^N$ and i.i.d. labels $\sigma^\mu \in \{0, 1\}$ with $\mu = 1, \dots, P$. The probability distribution of each component of a pattern is given by

$$P(\xi_{li}^\mu) = f_{\text{in}} \delta(\xi_{li}^\mu - 1) + (1 - f_{\text{in}}) \delta(\xi_{li}^\mu) \quad (\text{A3})$$

where f_{in} is the *input coding level* of the patterns. We consider a probability distribution of labels to be equal in form to (A3) but we allow the possibility to have different coding level in the output f_{out} .

In order to study the volume of synaptic weights that correctly associate to a given pattern of activity ξ^μ the corresponding label σ^μ we use a standard statistical mechanics approach [36, 59]. Firstly, we define the characteristic function

$$X_{\xi, \sigma}(W) = \prod_{\mu} \Theta \left(\frac{(2\sigma^\mu - 1)}{\sqrt{K}} \left(\sum_{l=1}^K c_l \tau_l^\mu - K\theta_s \right) - \kappa \right) \quad (\text{A4})$$

which is 1 when a given weight W_{li} correctly classifies all the patterns (we will call this a *solution*), and 0 otherwise. The volume of the allowed synapses, which in statistical mechanics is known as the *partition function*, is therefore:

$$Z = \int d\mu(W) X_{\xi,\sigma}(W) \quad (\text{A5})$$

where $d\mu(W)$ is the measure over the weights. We will consider in the following

$$\int d\mu(W) \bullet \equiv \int_0^\infty \prod_{li} dW_{li} \bullet \quad (\text{A6})$$

without giving constraints to the norm of the weights. As we will see the norm will be imposed self-consistently by the learning problem.

3. Replica method

To compute the average entropy $\langle \ln Z \rangle_{\xi,\sigma}$ of synaptic weights solutions in the large N limit, we resort the Replica Method [45] that is based on the following identity:

$$\langle \ln Z \rangle_{\xi,\sigma} = \lim_{n \rightarrow 0} \frac{\langle Z^n \rangle_{\xi,\sigma} - 1}{n} = \lim_{n \rightarrow 0} \frac{1}{n} \ln \langle Z^n \rangle_{\xi,\sigma}$$

This trick recondacts the problem of estimating the log of the partition function in (A5) to the computation of the average of n independent copies of the systems with the same realization of the disorder of the activity patterns and labels ξ^μ, σ^μ :

$$\langle Z^n \rangle = \left\langle \int \prod_{a=1}^n d\mu(W^a) \prod_{a,\mu} \theta \left(\frac{\sigma^\mu}{\sqrt{K}} \left(\sum_{l=1}^K c_l g \left(\sqrt{\frac{K}{N}} \sum_{i=1}^{N/K} W_{li}^a \xi_{li}^\mu - \sqrt{\frac{N}{K}} \theta_d \right) - K\theta_s \right) - \kappa \right) \right\rangle_{\xi,\sigma} \quad (\text{A7})$$

We will denote from now on a and b as the index that run over replicas $a, b = 1, \dots, n$. Notice also that, because of (A4) we can safely consider having labels $\sigma^\mu = \pm 1$ with the same output coding level as before. The computation follows standard steps [4, 59], which we will sketch here. Firstly we need to perform the average over the activity patterns ξ^μ ; we can do that by introducing the auxiliary variables

$$\lambda_l^{\mu a} = \sqrt{\frac{K}{N}} \sum_{i=1}^{N/K} W_{li} \xi_{li}^\mu - \sqrt{\frac{N}{K}} \theta_d \quad (\text{A8})$$

and the corresponding conjugated variables $\hat{\lambda}_l^{\mu a}$ that arise when we insert the integral representation of the Dirac delta function. The replicated partition function is

$$\begin{aligned} \langle Z^n \rangle &= \mathbb{E}_\sigma \int \prod_a d\mu(W^a) \int \prod_{\mu a l} \frac{d\lambda_l^{\mu a} d\hat{\lambda}_l^{\mu a}}{2\pi} e^{i\lambda_l^{\mu a} \hat{\lambda}_l^{\mu a}} \prod_{a,\mu} \theta \left(\frac{\sigma^\mu}{\sqrt{K}} \left(\sum_{l=1}^K c_l g(\lambda_l^{\mu a}) - K\theta_s \right) - \kappa \right) e^{i\sqrt{\frac{N}{K}} \theta_d \sum_{\mu a l} \lambda_l^{\mu a}} \\ &\times \prod_{li\mu} \left\langle e^{-i\xi_{li}^\mu \sqrt{\frac{K}{N}} \sum_a W_{li}^a \lambda_l^{\mu a}} \right\rangle_{\xi_{li}^\mu} \end{aligned} \quad (\text{A9})$$

The average over patterns can now be performed. In the large N limit, we can use the central limit theorem, having

$$\begin{aligned} \prod_{li\mu} \left\langle e^{-i\xi_{li}^\mu \sqrt{\frac{K}{N}} \sum_a W_{li}^a \lambda_l^{\mu a}} \right\rangle_{\xi_{li}^\mu} &= \prod_{li\mu} \left[1 - f_{\text{in}} + f_{\text{in}} e^{-i\sqrt{\frac{K}{N}} \sum_a W_{li}^a \lambda_l^{\mu a}} \right] \simeq \\ &= \prod_{li\mu} e^{-if_{\text{in}} \sqrt{\frac{K}{N}} \sum_a W_{li}^a \lambda_l^{\mu a} - \frac{f_{\text{in}}(1-f_{\text{in}})K}{2N} (\sum_a W_{li}^a \lambda_l^{\mu a})^2} \\ &= e^{-if_{\text{in}} \sqrt{\frac{K}{N}} \sum_{\mu a l} \hat{\lambda}_l^{\mu a} \sum_i W_{li}^a - \frac{f_{\text{in}}(1-f_{\text{in}})K}{N} \sum_{\mu l} \sum_{a < b} (\sum_i W_{li}^a W_{li}^b) \hat{\lambda}_l^{\mu a} \hat{\lambda}_l^{\mu b}} \\ &\times e^{-\frac{f_{\text{in}}(1-f_{\text{in}})K}{2N} \sum_{\mu a l} \sum_i (W_{li}^a \lambda_l^{\mu a})^2} \end{aligned} \quad (\text{A10})$$

By defining appropriate order parameters, it is possible to conveniently study the problem in the large- N limit. We define:

$$\sum_i W_{li}^a = \frac{N}{K} \bar{W} + \sqrt{\frac{N}{K}} M_l^a \quad (\text{A11a})$$

$$q_l^{ab} \equiv \frac{K}{N} \sum_i W_{li}^a W_{li}^b \quad (\text{A11b})$$

$$Q_l^a \equiv \frac{K}{N} \sum_i (W_{li}^a)^2 \quad (\text{A11c})$$

(A11a) represents the average synaptic weight; we expressed it in two contributions. The first one represents an averaged *scaled* synaptic weight

$$\bar{W} = \frac{\theta_d}{f_{\text{in}}} \quad (\text{A12})$$

justified by the fact that for each sub-perceptron of the first layer only $\frac{N}{K} f_{\text{in}}$ synapses contribute. The second term instead is a $\sqrt{\frac{N}{K}}$ correction that is needed in order to fine tune the average synaptic weight relatively to the threshold θ_d .

The quantity q_l^{ab} is the overlap between the weights of two different replicas a and b belonging to the same dendritic branch l , while Q_l^a represents the averaged squared norm of a synaptic weight belonging to dendritic branch l .

Enforcing the definitions (A11) in (A9), by using Dirac delta functions, we can express the replicated partition function as an integration over the order parameters $q_l^{ab}, \hat{q}, Q, \hat{Q}, M, \hat{M}$:

$$\begin{aligned} \langle Z^n \rangle_{\xi, \sigma} = & \int \prod_{a < b, l} \frac{dq_l^{ab} d\hat{q}_l^{ab}}{2\pi K/N} \int \prod_{a, l} \frac{dQ_l^a d\hat{Q}_l^a}{2\pi K/N} \int \prod_{a, l} \frac{dM_l^a d\hat{M}_l^a}{2\pi \sqrt{K/N}} e^{-\frac{N}{K} \sum_{a < b, l} q_l^{ab} \hat{q}_l^{ab} - \frac{N}{K} \sum_{a, l} Q_l^a \hat{Q}_l^a - \frac{N}{K} \bar{W} \sum_{a, l} \hat{M}_l^a} \\ & \times e^{\frac{N}{K} G_S(\hat{q}_l^{ab}, \hat{Q}_l^a, \hat{M}_l^a) + N \alpha G_E(q_l^{ab}, Q_l^a, M_l^a)}. \end{aligned} \quad (\text{A13})$$

where we collected the entropic contribution G_S and the energetic one G_E . The first is the usual term that counts how many coupling vectors W^a fulfill the constraints (A11); the second is specific to the learning rule which is used, and depends on the Heaviside function that counts learned patterns:

$$G_S(\hat{q}_l^{ab}, \hat{Q}_l^a, \hat{M}_l^a) = \ln \int_0^\infty \prod_{a, l} dW_l^a e^{\sum_{a < b, l} \hat{q}_l^{ab} W_l^a W_l^b + \sum_{a, l} \hat{Q}_l^a (W_l^a)^2 + \sum_{a, l} \hat{M}_l^a W_l^a} \quad (\text{A14a})$$

$$\begin{aligned} G_E(q_l^{ab}, Q_l^a, M_l^a) = & \ln \mathbb{E}_\sigma \int \prod_{a, l} \frac{d\lambda_l^a d\hat{\lambda}_l^a}{2\pi} \Theta \left(\frac{\sigma}{\sqrt{K}} \left(\sum_l c_l g(\lambda_l^a) - K\theta_s \right) - \kappa \right) e^{i \sum_{a, l} \lambda_l^a \hat{\lambda}_l^a - f_{\text{in}}(1-f_{\text{in}}) \sum_{a < b, l} q_l^{ab} \hat{\lambda}_l^a \hat{\lambda}_l^b} \\ & \times e^{-\frac{f_{\text{in}}(1-f_{\text{in}})}{2} \sum_{a, l} Q_l^a (\hat{\lambda}_l^a)^2 - i f_{\text{in}} \sum_{a, l} M_l^a \hat{\lambda}_l^a}. \end{aligned} \quad (\text{A14b})$$

We can now evaluate in the large N limit (A13) using the saddle point method. In order to restrict the space where to search saddle points we proceed by assuming a particular form of the order parameters, which is the main topic of the next section.

4. Replica Symmetric analysis

We use a Replica Symmetric (RS) ansatz, i.e. we assume that the order parameters do not depend on the replica indexes and of the index corresponding to the dendritic branch:

$$q_l^{ab} = q, \quad Q_l^a = Q, \quad M_l^a = M, \quad (\text{A15a})$$

$$\hat{q}_l^{ab} = \hat{q}, \quad \hat{Q}_l^a = \hat{Q}, \quad \hat{M}_l^a = \hat{M} \quad (\text{A15b})$$

In the RS ansatz and in the small n limit, using *Hubbard-Stratonovich* transformations:

$$e^{\frac{1}{2}bx^2} = \int \frac{dz}{\sqrt{2\pi}} e^{-\frac{z^2}{2} + \sqrt{b}xz},$$

the entropic and energetic terms are the following

$$\mathcal{G}_S \equiv \lim_{n \rightarrow 0} \frac{1}{nK} G_S(\hat{q}, \hat{Q}, \hat{M}) = \ln \sqrt{\frac{2\pi}{\hat{q} - 2\hat{Q}}} + \frac{1}{2} \left(\frac{\hat{M}^2 + \hat{q}}{\hat{q} - 2\hat{Q}} \right) + \int Dz \ln H \left(-\frac{\hat{M} + \sqrt{\hat{q}z}}{\sqrt{\hat{q} - 2\hat{Q}}} \right) \quad (\text{A16a})$$

$$\mathcal{G}_E \equiv \lim_{n \rightarrow 0} \frac{G_E(q, Q, M)}{n} = \mathbb{E}_\sigma \int \prod_l Dt_l \ln \left[\int \prod_l D\lambda_l \Theta \left(\frac{\sigma}{\sqrt{K}} \left(\sum_l c_l g \left(\sqrt{f_{\text{in}}(1 - f_{\text{in}})(Q - q)} \lambda_l + a_l \right) - K\theta_s \right) - \kappa \right) \right] \quad (\text{A16b})$$

where we have introduced the variable

$$a_l \equiv f_{\text{in}}M + \sqrt{f_{\text{in}}(1 - f_{\text{in}})q} t_l \quad (\text{A17})$$

for convenience. In (A16a) we have also introduced $H(x) \equiv \int_x^\infty Dz = \frac{1}{2} \text{Erfc} \left(\frac{x}{\sqrt{2}} \right)$ and $Dz \equiv G(z) dz$ with $G(z)$ being a standard normal Gaussian $G(z) = \exp(-z^2/2)/\sqrt{2\pi}$.

a. Large K limit

We focus on the limit $K \rightarrow \infty$ (with $\frac{K}{N} \rightarrow 0$), for two main reasons:

- on the analytical level, it allows to simplify the numerical evaluation of the saddle point equations corresponding to the RS ansatz;
- it is *biologically* realistic: the number of dendritic branches in neurons is typically large (in some cases even more than a hundred, REF) and the number of synapses in each branch is typically large as well (REFS?).

To evaluate this limit, we need to do some manipulations on the energetic contribution (A16b) which are based on the central limit theorem. Let us first consider the term in square brackets:

$$\begin{aligned} I &= \int \prod_l D\lambda_l \Theta \left(\frac{\sigma}{\sqrt{K}} \left(\sum_l c_l g \left(\sqrt{f_{\text{in}}(1 - f_{\text{in}})(Q - q)} \lambda_l + a_l \right) - K\theta_s \right) - \kappa \right) \\ &= \int \frac{dh d\hat{h}}{2\pi} e^{-ih\hat{h}} \Theta \left[\sigma \left(h - \sqrt{K}\theta_s \right) - \kappa \right] \int \prod_l D\lambda_l e^{\frac{i\hat{h}}{\sqrt{K}} \sum_l c_l g \left(a_l + \sqrt{f_{\text{in}}(1 - f_{\text{in}})(Q - q)} \lambda_l \right)} \end{aligned} \quad (\text{A18})$$

In the large K limit we can therefore expand the exponential up to second order

$$\begin{aligned} I &\simeq \int \frac{dh d\hat{h}}{2\pi} e^{-ih\hat{h}} \Theta \left(\sigma \left(h - \sqrt{K}\theta_s \right) - \kappa \right) \int \prod_l D\lambda_l \left[1 + \frac{i\hat{h}}{\sqrt{K}} \sum_l c_l g \left(a_l + \sqrt{f_{\text{in}}(1 - f_{\text{in}})(Q - q)} \lambda_l \right) + \right. \\ &\quad \left. - \frac{\hat{h}^2}{2K} \left(\sum_l c_l g \left(a_l + \sqrt{f_{\text{in}}(1 - f_{\text{in}})(Q - q)} \lambda_l \right) \right)^2 \right]. \end{aligned} \quad (\text{A19})$$

and we can integrate with respect to all the λ_l variables term by term. Exponentiating the expression again and integrating over \hat{h} we get

$$I = \int Dh \Theta \left(\sigma \left(M^{(0)} + \sqrt{\Delta^{(0)}} h - \sqrt{K}\theta_s \right) - \kappa \right) \quad (\text{A20})$$

where we have introduced the variables:

$$M^{(0)} = \frac{1}{\sqrt{K}} \sum_l c_l \langle g \rangle_\lambda \quad (\text{A21a})$$

$$D^{(0)} = \frac{1}{K} \sum_l c_l^2 [\langle g^2 \rangle_\lambda - \langle g \rangle_\lambda^2]. \quad (\text{A21b})$$

and the notation

$$\langle g \rangle_\lambda = \int D\lambda g \left(f_{\text{in}} M + \sqrt{f_{\text{in}}(1-f_{\text{in}})} q t_l + \sqrt{f_{\text{in}}(1-f_{\text{in}})} (Q-q) \lambda \right). \quad (\text{A22})$$

Using again the central limit theorem for the K integrals over the variable t_l we get:

$$\mathcal{G}_E = \mathbb{E}_\sigma \int Dt \ln \int D\lambda \Theta \left[\sigma \left(M_0 + \sqrt{D_0} t + \sqrt{D_1} \lambda - \sqrt{K} \theta_s \right) - \kappa \right] \quad (\text{A23})$$

where:

$$M_0 = \frac{1}{\sqrt{K}} \sum_l c_l \langle g \rangle_{\lambda,t} = m_c \langle g \rangle_{\lambda,t} \quad (\text{A24a})$$

$$D_0 = \frac{1}{K} \sum_l c_l^2 [\langle \langle g \rangle_\lambda^2 \rangle_t - \langle \langle g \rangle_\lambda \rangle_t^2] = w_c [\langle \langle g \rangle_\lambda^2 \rangle_t - \langle \langle g \rangle_\lambda \rangle_t^2] \quad (\text{A24b})$$

$$D_1 = w_c [\langle \langle g^2 \rangle_\lambda \rangle_t - \langle \langle g \rangle_\lambda^2 \rangle_t] \quad (\text{A24c})$$

and for example

$$\langle \langle g \rangle_\lambda \rangle_t = \int Dt D\lambda g \left(f_{\text{in}} M + \sqrt{f_{\text{in}}(1-f_{\text{in}})} q t + \sqrt{f_{\text{in}}(1-f_{\text{in}})} (Q-q) \lambda \right). \quad (\text{A25})$$

Using the definition of the committee machine in which all weights in the second layer are s.t. $c_l = 1$, we have $m_c = \sqrt{K}$ and $w_c = 1$. In order to have a well-defined large K limit we have to impose (analogously to what we have done on the dendritic threshold θ_d) that the divergence induced by the somatic threshold θ_s cancels with the one coming from M_0 . We therefore impose that M scales, in the large K limit, as

$$M = \bar{M} + \frac{\delta M}{\sqrt{K}}. \quad (\text{A26})$$

M_0 can be simplified by making a rotation over the integration measures λ and t

$$\begin{aligned} M_0 &= \sqrt{K} \langle \langle g \rangle_\lambda \rangle_t = \sqrt{K} \int D\lambda Dt g \left(\sqrt{f_{\text{in}}(1-f_{\text{in}})} q t + \sqrt{f_{\text{in}}(1-f_{\text{in}})} (Q-q) \lambda + f_{\text{in}} M \right) \\ &= \sqrt{K} \int D\lambda g \left(\sqrt{f_{\text{in}}(1-f_{\text{in}})} Q \lambda + f_{\text{in}} M \right) \end{aligned} \quad (\text{A27})$$

We can now insert the scaling in (A26)

$$\begin{aligned} M_0 &= \sqrt{K} \int D\lambda g \left(\sqrt{f_{\text{in}}(1-f_{\text{in}})} Q \lambda + f_{\text{in}} M \right) \\ &\simeq \sqrt{K} \int D\lambda g \left(\sqrt{f_{\text{in}}(1-f_{\text{in}})} Q \lambda + f_{\text{in}} \bar{M} \right) + f_{\text{in}} \delta M \int D\lambda g' \left(\sqrt{f_{\text{in}}(1-f_{\text{in}})} Q \lambda + f_{\text{in}} \bar{M} \right) \\ &= \sqrt{K} \theta_s + \Delta \end{aligned} \quad (\text{A28})$$

Therefore, \bar{M} is fixed by the relation:

$$\theta_s = \int Dy g \left(\sqrt{f_{\text{in}}(1-f_{\text{in}})} Q y + f_{\text{in}} \bar{M} \right), \quad (\text{A29})$$

that involves the output threshold. Hence the energetic term (A23) becomes:

$$\mathcal{G}_E = \mathbb{E}_\sigma \int Dz \ln H \left(\frac{\kappa - \sigma \Delta + \sqrt{D_0} z}{\sqrt{D_1}} \right) = \int Dz \left[f_{\text{out}} \ln H \left(\frac{\kappa - \Delta + \sqrt{D_0} z}{\sqrt{D_1}} \right) + (1 - f_{\text{out}}) \ln H \left(\frac{\kappa + \Delta + \sqrt{D_0} z}{\sqrt{D_1}} \right) \right] \quad (\text{A30})$$

where the order parameters, strictly dependent on the choice of the activation function $g(x)$, are simplified as:

$$\begin{aligned}\Delta &\equiv f_{\text{in}} M \int Dx g' \left(\sqrt{f_{\text{in}}(1-f_{\text{in}})Q} x + f_{\text{in}} \overline{M} \right) \\ D_0 &= \Delta_q - \Delta_0 \\ D_1 &= \Delta_Q - \Delta_q\end{aligned}$$

where we have renamed δM by M with a slight abuse of notation. We have also defined the generic “effective order parameter” or *kernel* functions

$$\Delta_q = \int Dx \left[\int Dy g \left(\sqrt{f_{\text{in}}(1-f_{\text{in}})q} x + \sqrt{f_{\text{in}}(1-f_{\text{in}})(Q-q)} y + f_{\text{in}} \overline{M} \right) \right]^2 \quad (\text{A32})$$

Δ_Q and Δ_0 being obtained by simply substituting in the previous expression $q \rightarrow Q$ and $q \rightarrow 0$ respectively. We report them here for clarity

$$\Delta_Q = \int Dx g^2 \left(\sqrt{f_{\text{in}}(1-f_{\text{in}})Q} x + f_{\text{in}} \overline{M} \right), \quad (\text{A33a})$$

$$\Delta_0 = \left[\int Dy g \left(\sqrt{f_{\text{in}}(1-f_{\text{in}})Q} y + f_{\text{in}} \overline{M} \right) \right]^2. \quad (\text{A33b})$$

We have called Δ_q an *effective order parameter* since (A30) (and therefore the whole quenched entropy) is perfectly equivalent to the one found in the perceptron model studied by Brunel in a series of papers [32, 38], but where order parameters q and Q are substituted respectively by $\Delta_q - \Delta_0$ and $\Delta_Q - \Delta_0$.

b. Free entropy and saddle point equations

The average *free entropy* of the dendritic model of a neuron is therefore

$$\phi = \lim_{N \rightarrow \infty} \frac{1}{N} \langle \ln Z \rangle_{\xi, \sigma} = \frac{q\hat{q}}{2} - Q\hat{Q} - \overline{W}\hat{M} + \mathfrak{G}_S + \alpha \mathfrak{G}_E \quad (\text{A34})$$

We now need to compute the saddle point equations by differentiating (A34) with respect to the order parameters $Q, q, M, \hat{Q}, \hat{q}, \hat{M}$. The saddle point equations involving the entropic term (i.e. taking derivatives with respect to \hat{M} , \hat{Q} and \hat{q}) are the same as in the case of the perceptron

$$\overline{W} = \int Dz \frac{\int_0^\infty dW W e^{-(\hat{q}-2\hat{Q})\frac{W^2}{2} + (\hat{M} + \sqrt{\hat{q}z})W}}{\int_0^\infty dW e^{-(\hat{q}-2\hat{Q})\frac{W^2}{2} + (\hat{M} + \sqrt{\hat{q}z})W}} \quad (\text{A35a})$$

$$Q = \int Dz \frac{\int_0^\infty dW W^2 e^{-(\hat{q}-2\hat{Q})\frac{W^2}{2} + (\hat{M} + \sqrt{\hat{q}z})W}}{\int_0^\infty dW e^{-(\hat{q}-2\hat{Q})\frac{W^2}{2} + (\hat{M} + \sqrt{\hat{q}z})W}} \quad (\text{A35b})$$

$$q = \int Dz \frac{\int_0^\infty dW \left(W^2 - \frac{zW}{\sqrt{\hat{q}}} \right) e^{-(\hat{q}-2\hat{Q})\frac{W^2}{2} + (\hat{M} + \sqrt{\hat{q}z})W}}{\int_0^\infty dW e^{-(\hat{q}-2\hat{Q})\frac{W^2}{2} + (\hat{M} + \sqrt{\hat{q}z})W}} = \int Dz \left[\frac{\int_0^\infty dW W e^{-(\hat{q}-2\hat{Q})\frac{W^2}{2} + (\hat{M} + \sqrt{\hat{q}z})W}}{\int_0^\infty dW e^{-(\hat{q}-2\hat{Q})\frac{W^2}{2} + (\hat{M} + \sqrt{\hat{q}z})W}} \right]^2 \quad (\text{A35c})$$

In order to express the remaining saddle point equations in a compact way, we define the quantities:

$$\begin{aligned}a_\sigma(z) &= \frac{\sqrt{D_0}z - \sigma\Delta + \kappa}{\sqrt{D_1}} = \sqrt{\frac{D_0}{D_1}}(z - \tau_\sigma) \\ \tau_\sigma &= \frac{\sigma\Delta - \kappa}{\sqrt{D_0}}.\end{aligned}$$

Deriving (A34) with respect to M , Q and q lead respectively to

$$0 = \mathbb{E}_\sigma \sigma \int Dz \frac{G(a_\sigma(z))}{H(a_\sigma(z))} \quad (\text{A37a})$$

$$\hat{Q} = \frac{\alpha}{2} \mathbb{E}_\sigma \int Dz \frac{G(a_\sigma(z))}{H(a_\sigma(z))} \left[\frac{a_\sigma(z)}{D_1} \frac{dD_1}{dQ} - \frac{z}{\sqrt{D_0 D_1}} \frac{dD_0}{dQ} \right] \quad (\text{A37b})$$

$$\hat{q} = \alpha \mathbb{E}_\sigma \int Dz \frac{G(a_\sigma(z))}{H(a_\sigma(z))} \left[-\frac{a_\sigma(z)}{D_1} \frac{dD_1}{dq} + \frac{z}{\sqrt{D_0 D_1}} \frac{dD_0}{dq} \right] \quad (\text{A37c})$$

where we used the saddle point equation (A37a) when performing the derivative in Q^1 . The six saddle points Eqs. ((A35a), A35b, A35c, A37a, A37b, A37c), obtained in the large $K, N \rightarrow \infty$ limit with $N \gg K$, have to be numerically solved to obtain the values of the order parameters and represent the final result of our RS analysis.

Notice that imposing $g(x) = x$ we recover the previous saddle point expressions obtained for the simple linear neuron model [32, 38]. Notice also that in the case $f_{\text{out}} = \frac{1}{2}$ saddle point equation (A37a) gives $M = 0$; in this case therefore $\tau_\sigma = 0$.

c. Effective order parameters for some non-linearities

We report here the analytical expressions of the effective order parameters for several non-linearities of interest

- *Recovering the one-layer neuron model:* if we impose $g(x) = x$ we recover the one-layer neuron model. We report here the expressions of the corresponding effective order parameters for convenience

$$\Delta = f_{\text{in}} M \quad (\text{A38a})$$

$$\Delta_q = f_{\text{in}}(1 - f_{\text{in}})q + f_{\text{in}}^2 \overline{M}^2 \quad (\text{A38b})$$

and, in particular

$$\Delta_Q = f_{\text{in}}(1 - f_{\text{in}})Q + f_{\text{in}}^2 \overline{M}^2 \quad (\text{A39a})$$

$$\Delta_0 = f_{\text{in}}^2 \overline{M}^2 \quad (\text{A39b})$$

As a result \overline{M} does not appear anywhere in the energetic term of equation (A30), and $\theta_s = f_{\text{in}} \overline{M}$ is also irrelevant.

- *Theta non-linearity:* $g(x) = \Theta(x)$.

To evaluate the integrals it is useful to use the following identity

$$\int Dz H^2(a + bz) = H\left(\frac{a}{\sqrt{1+b^2}}\right) - 2T\left(\frac{a}{\sqrt{1+b^2}}, \frac{1}{\sqrt{1+2b^2}}\right) \quad (\text{A40})$$

where T is the Owen's T function defined as

$$T(h, s) \equiv \frac{1}{2\pi} \int_0^s dx \frac{e^{-(1+x^2)\frac{h^2}{2}}}{1+x^2}, \quad (\text{A41})$$

and has the following important properties

$$T(h, s) \simeq \frac{G(h)s}{\sqrt{2\pi}} + O(s^2) \quad \text{for } s \rightarrow 0 \quad (\text{A42a})$$

$$T(h, 1) = \frac{1}{2} H(h)H(-h) \quad (\text{A42b})$$

where we remind that $G(x)$ is the Gaussian with mean zero and unit variance. Defining the quantity

$$M_\star = \frac{f_{\text{in}} \overline{M}}{\sqrt{f_{\text{in}}(1 - f_{\text{in}})Q}} \quad (\text{A43})$$

¹ this is why no derivative with respect to Q of Δ compares in (A37b)

the effective order parameters for the theta non-linearity are

$$\Delta = M_\star G(-M_\star) \quad (\text{A44a})$$

$$\Delta_q = H(-M_\star) - 2T \left(M_\star, \sqrt{\frac{Q-q}{Q+q}} \right) \quad (\text{A44b})$$

and, in particular

$$\Delta_Q = H(-M_\star), \quad (\text{A45a})$$

$$\Delta_0 = H(-M_\star)^2. \quad (\text{A45b})$$

\bar{M} is fixed by the relation

$$\theta_s = H(-M_\star). \quad (\text{A46})$$

- *ReLU non-linearity*: $g(x) = x\Theta(x)$ We have

$$\Delta = f_{\text{in}} M H(-M_\star) \quad (\text{A47a})$$

$$\begin{aligned} \Delta_q &= f_{\text{in}}(1-f_{\text{in}})(Q-q) \sqrt{\frac{Q-q}{Q+q}} G^2 \left(\frac{f_{\text{in}} \bar{M}}{\sqrt{f_{\text{in}}(1-f_{\text{in}})(Q+q)}} \right) \\ &\quad + f_{\text{in}} \left((1-f_{\text{in}})q + f_{\text{in}} \bar{M}^2 \right) \left[H(-M_\star) - 2T \left(-M_\star, \sqrt{\frac{Q-q}{Q+q}} \right) \right] \\ &\quad + 2f_{\text{in}} \bar{M} \sqrt{f_{\text{in}}(1-f_{\text{in}})Q} G(M_\star) H \left(-M_\star \sqrt{\frac{Q-q}{Q+q}} \right) + 2f_{\text{in}}(1-f_{\text{in}})q \sqrt{\frac{Q-q}{Q+q}} G(M_\star) G \left(M_\star \sqrt{\frac{Q-q}{Q+q}} \right) \end{aligned} \quad (\text{A47b})$$

and in particular

$$\Delta_Q = f_{\text{in}} \left((1-f_{\text{in}})Q + f_{\text{in}} \bar{M}^2 \right) H(-M_\star) + f_{\text{in}} \bar{M} \sqrt{f_{\text{in}}(1-f_{\text{in}})Q} G(-M_\star), \quad (\text{A48a})$$

$$\Delta_0 = \left[\sqrt{f_{\text{in}}(1-f_{\text{in}})Q} G(M_\star) + f_{\text{in}} \bar{M} H(-M_\star) \right]^2 \quad (\text{A48b})$$

Note that \bar{M} is fixed by the relation

$$\theta_s = \sqrt{f_{\text{in}}(1-f_{\text{in}})Q} G(M_\star) + f_{\text{in}} \bar{M} H(-M_\star) \quad (\text{A49})$$

d. Small data regime

In the $\alpha \rightarrow 0$ limit the saddle point equations can be solved exactly. Indeed $\hat{q} = \hat{Q} = 0$ and equations (A35a), (A35b), (A35c) give respectively

$$\bar{W} = \frac{\theta_d}{f_{\text{in}}} = \frac{\int_0^\infty dW W e^{\hat{M}W}}{\int_0^\infty dW e^{\hat{M}W}} = -\frac{1}{\hat{M}} \quad (\text{A50a})$$

$$Q = \frac{\int_0^\infty dW W^2 e^{\hat{M}W}}{\int_0^\infty dW e^{\hat{M}W}} = \frac{2}{\hat{M}^2} \quad (\text{A50b})$$

$$q = \left[\frac{\int_0^\infty dW W e^{\hat{M}W}}{\int_0^\infty dW e^{\hat{M}W}} \right]^2 = \frac{1}{\hat{M}^2} \quad (\text{A50c})$$

e. Distribution of dendritic preactivations

We derive here the distribution of dendritic preactivations after learning. Since the each dendritic branch has access to an independent portion of the input, the distribution of the preactivations is factorized over the K dendritic

branches. In the large K limit the distribution tends to a Gaussian $\mathcal{N}(\mu, \sigma)$ as can be inspected from the post activation mean (A29) and from the argument of the kernel functions (A32). Denoting by $\lambda_l \equiv \sqrt{\frac{K}{N}} \sum_{i=1}^{N/K} W_{li} \xi_{li} - \sqrt{\frac{N}{K}} \theta_d$ as in the main text, the mean and the variance of the distribution of the l -th dendritic branch are respectively

$$\mu = \mathbb{E}_{\xi} \lambda_l = f_{\text{in}} \bar{M} \quad (\text{A51a})$$

$$\sigma^2 = \mathbb{E}_{\xi} \lambda_l^2 - \mu^2 = f_{\text{in}}(1 - f_{\text{in}})Q \quad (\text{A51b})$$

as confirmed by (A29).

In the $\alpha \rightarrow 0$ the variance above can be expressed explicitly in terms of θ_d and f_{in} thanks to (A50a) and (A50b). We get that the standard deviation of the dendritic preactivation depends linearly on the dendritic inhibition threshold

$$\sigma = \theta_d \sqrt{\frac{2(1 - f_{\text{in}})}{f_{\text{in}}}}. \quad (\text{A52})$$

We checked that this linear relation is satisfied even at finite α , or considering a different distribution over the weights at initialization, see below. This shows that if θ_d is small one does not completely use the non-linearity and the model behaves like a one-layer model.

f. Limit of large somatic thresholds

When the somatic threshold θ_s diverges, the only way to satisfy (A29) is that \bar{M} diverges if the non-linearity g is unbounded. This can be inspected already in (A49) in the case of the ReLU non-linearity.

Instead if the non-linearity is bounded, the right hand side of (A29) is a bounded function of \bar{M} as well, therefore above a certain critical value of θ_s it will not be possible to find the corresponding value of \bar{M} .

Moreover, if the non-linearity diverges linearly for large arguments, we expect to recover back the free energy and the expressions for the one-layer neuron model for large θ_s . Indeed expanding equation (A29) one finds $\bar{M} \sim \theta_s / f_{\text{in}}$ and the effective order parameters reduce to those ones of the perceptron, see (A38).

5. Critical capacity

In this section we show how in our formalism, it is possible to compute the maximal number of inputs that the neuron is able to classify. We underline that this can be done for a generic form of dendritic non-linearity.

In the critical capacity limit, the set of possible synaptic weights shrinks towards a single point and q tends to Q :

$$q = Q - dq. \quad (\text{A53})$$

Correspondingly, the other order parameters scale as

$$\hat{q}, \hat{Q} \sim \frac{C}{dq^2} \quad (\text{A54a})$$

$$\hat{q} - 2\hat{Q} \sim \frac{A}{dq} \quad (\text{A54b})$$

$$\hat{M} \sim -\frac{B\sqrt{C}}{dq} \quad (\text{A54c})$$

Using the identities (where a is a positive constant)

$$\frac{\int_0^\infty dx x e^{-a\frac{x^2}{2} + bx}}{\int_0^\infty dx e^{-a\frac{x^2}{2} + bx}} = \frac{b}{a} + \frac{1}{\sqrt{a}} \frac{G\left(-\frac{b}{\sqrt{a}}\right)}{H\left(-\frac{b}{\sqrt{a}}\right)} \quad (\text{A55a})$$

$$\frac{\int_0^\infty dx x^2 e^{-a\frac{x^2}{2} + bx}}{\int_0^\infty dx e^{-a\frac{x^2}{2} + bx}} = \frac{1}{a} + \frac{b^2}{a^2} + \frac{b}{a^{3/2}} \frac{G\left(-\frac{b}{\sqrt{a}}\right)}{H\left(-\frac{b}{\sqrt{a}}\right)} \quad (\text{A55b})$$

and the expansion

$$\frac{G(x)}{H(x)} \simeq x\theta(x), \quad \text{for } |x| \gg 1, \quad (\text{A56})$$

the saddle point equations (A35) can be written as

$$\bar{W} = \frac{\sqrt{C}}{A} [G(B) - BH(B)] \quad (\text{A57a})$$

$$Q = \frac{C}{A^2} [(1 + B^2)H(B) - BG(B)] \quad (\text{A57b})$$

$$A = H(B). \quad (\text{A57c})$$

More work is required to derive the asymptotic limit of equations (A37). First of all we need the expansion of the effective order parameters

$$D_0 = \Delta_q - \Delta_0 = \Delta_Q - \Delta_0 - D_1 \simeq \Gamma_0 - \Gamma_1 dq \quad (\text{A58a})$$

$$D_1 = \Delta_Q - \Delta_q = \Gamma_1 dq + O(dq^2) \quad (\text{A58b})$$

where we have defined

$$\Gamma_0 = \Delta_Q - \Delta_0 = \int Dx g^2 \left(\sqrt{f_{\text{in}}(1 - f_{\text{in}})Q} x + f_{\text{in}}\bar{M} \right) - \left[\int Dy g \left(\sqrt{f_{\text{in}}(1 - f_{\text{in}})Q} y + f_{\text{in}}\bar{M} \right) \right]^2 \quad (\text{A59a})$$

$$\Gamma_1 = f_{\text{in}}(1 - f_{\text{in}}) \int Dz \left[g' \left(\sqrt{f_{\text{in}}(1 - f_{\text{in}})Q} z + f_{\text{in}}\bar{M} \right) \right]^2 \quad (\text{A59b})$$

Now we subtract (A37b) with (A37c) getting

$$\begin{aligned} \hat{q} - 2\hat{Q} &= \alpha \mathbb{E}_\sigma \int Dz \frac{G(a_\sigma(z))}{H(a_\sigma(z))} \left[\frac{z}{\sqrt{D_0 D_1}} \left(\frac{dD_0}{dq} + \frac{dD_0}{dQ} \right) - \frac{a_\sigma(z)}{D_1} \left(\frac{dD_1}{dq} + \frac{dD_1}{dQ} \right) \right] \\ &= \alpha \mathbb{E}_\sigma \int Dz \frac{G(a_\sigma(z))}{H(a_\sigma(z))} \left[\frac{z}{\sqrt{D_0 D_1}} \frac{d\Gamma_0}{dQ} - \frac{a_\sigma(z)}{D_1} \frac{d\Gamma_1}{dQ} dq \right] \end{aligned} \quad (\text{A60})$$

Similarly (A37c) becomes

$$\hat{q} = \alpha \mathbb{E}_\sigma \int Dz \frac{G(a_\sigma(z))}{H(a_\sigma(z))} \left[-\frac{a_\sigma(z)}{D_1} \frac{dD_1}{dq} \right] \quad (\text{A61})$$

because the second term in (A37c) is subleading in dq . Using the expansion (A56) and the identities

$$\int Dz z^2 \Theta(z - \tau_\sigma) = H(\tau_\sigma) + \tau_\sigma G(\tau_\sigma) \quad (\text{A62a})$$

$$\int Dz z \Theta(z - \tau_\sigma) = G(\tau_\sigma) \quad (\text{A62b})$$

we obtain the following saddle point equations

$$0 = \mathbb{E}_\sigma \sigma [G(\tau_\sigma) - \tau_\sigma H(\tau_\sigma)] \quad (\text{A63a})$$

$$A = \alpha_c \left[\frac{1}{\Gamma_1} \frac{d\Gamma_0}{dQ} \mathbb{E}_\sigma H(\tau_\sigma) - \frac{\Gamma_0}{\Gamma_1^2} \frac{d\Gamma_1}{dQ} \mathbb{E}_\sigma [(1 + \tau_\sigma^2)H(\tau_\sigma) - \tau_\sigma G(\tau_\sigma)] \right] \quad (\text{A63b})$$

$$C = \frac{\alpha_c \Gamma_0}{\Gamma_1} \mathbb{E}_\sigma [(1 + \tau_\sigma^2)H(\tau_\sigma) - \tau_\sigma G(\tau_\sigma)], \quad (\text{A63c})$$

which involve the critical capacity as an unknown parameter to find. Notice that in the previous equation we have redefined $\tau_\sigma = (\sigma\Delta - \kappa)/\sqrt{\Gamma_0}$. The full set of saddle point equations for the order parameters A, B, C, M, Q, \bar{M} and for α_c are

$$\bar{W} = \frac{\sqrt{C}}{A} [G(B) - BH(B)] \quad (\text{A64a})$$

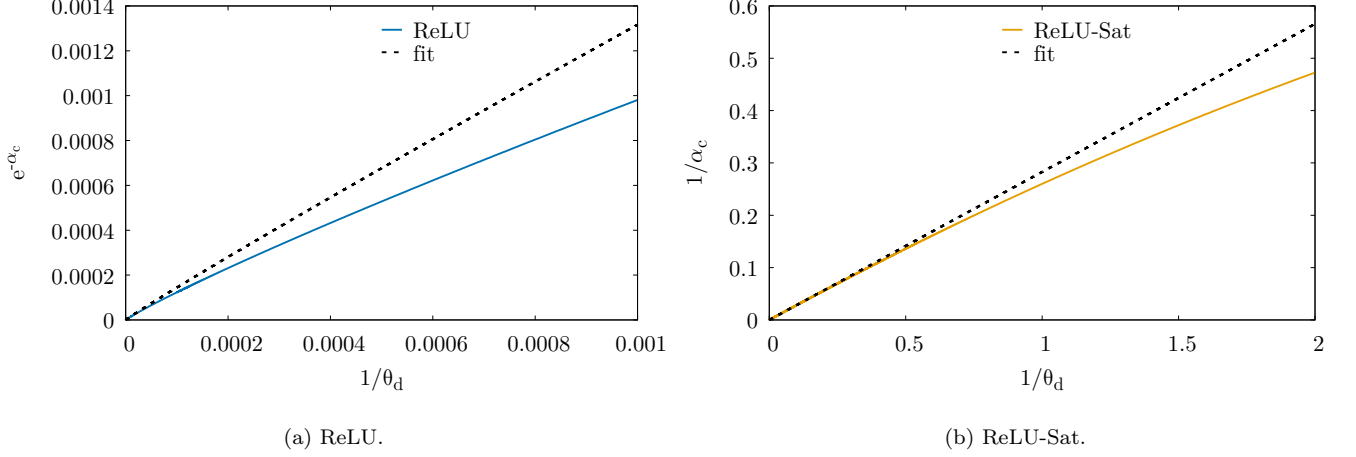


Figure 10. Fit to the critical capacity for large dendritic thresholds for the ReLU (left panel) and the ReLU-Sat (right panel) nonlinearities. The external parameters are the same used in the corresponding figures of the main text, i.e. $f_{\text{in}} = f_{\text{out}} = \theta_s = 0.5$ and $\kappa = 0$. Notice that in the case of the ReLU function (left panel) we are plotting $e^{-\alpha_c}$ versus θ_d at variance to the ReLU-Sat. In each plot the dashed black line represents a linear fit $a + bx$ of the analytical data for large θ_d .

$$Q = \frac{C}{A^2} [(1 + B^2) H(B) - BG(B)] \quad (\text{A64b})$$

$$A = H(B) \quad (\text{A64c})$$

$$0 = \mathbb{E}_\sigma \sigma [G(\tau_\sigma) - \tau_\sigma H(\tau_\sigma)] \quad (\text{A64d})$$

$$A = \frac{\alpha_c}{\Gamma_1} \frac{d\Gamma_0}{dQ} \mathbb{E}_\sigma H(\tau_\sigma) - \frac{1}{\Gamma_1} \frac{d\Gamma_1}{dQ} C \quad (\text{A64e})$$

$$C = \frac{\alpha_c \Gamma_0}{\Gamma_1} \mathbb{E}_\sigma [(1 + \tau_\sigma^2) H(\tau_\sigma) - \tau_\sigma G(\tau_\sigma)] \quad (\text{A64f})$$

$$\theta_s = \int Dy g \left(\sqrt{f_{\text{in}}(1 - f_{\text{in}})Q} y + f_{\text{in}} \bar{M} \right). \quad (\text{A64g})$$

As we have anticipated before, in the case $f_{\text{out}} = 0.5$ the equations can be further simplified, since $M = 0$; if also $\kappa = 0$ therefore $\tau_\sigma = 0$; the saddle point equations (A64) then reduce to

$$\bar{W} = \sqrt{\frac{\alpha_c \Gamma_0}{2\Gamma_1}} \frac{1}{H(B)} [G(B) - BH(B)] \quad (\text{A65a})$$

$$Q = \frac{\alpha_c \Gamma_0}{2\Gamma_1} \frac{1}{H^2(B)} [(1 + B^2) H(B) - BG(B)] \quad (\text{A65b})$$

$$\alpha_c = \frac{2\Gamma_1 H(-B)}{\frac{d\Gamma_0}{dQ} - \frac{\Gamma_0}{\Gamma_1} \frac{d\Gamma_1}{dQ}} \quad (\text{A65c})$$

$$\theta_s = \int Dy g \left(\sqrt{f_{\text{in}}(1 - f_{\text{in}})Q} y + f_{\text{in}} \bar{M} \right). \quad (\text{A65d})$$

a. Limit of large dendritic threshold

As mentioned in the main text, the critical capacity of the model depends strongly on the shape of the non-linearity. In particular, in the limit of large dendritic threshold the critical capacity can diverge differently depending if the non-linearity saturates or not for a sufficiently large stimulus. We show in Fig. 10 how the critical capacity diverges logarithmically in θ_d for the ReLU activation function whereas the divergence is linear in the ReLU-Sat activation function. Performing a fit we get when $\theta_d \rightarrow \infty$

$$\alpha_c^{\text{ReLU-Sat}} \simeq 3.518 \theta_d \quad (\text{A66a})$$

$$\alpha_c^{\text{ReLU}} \simeq 0.9602 \ln \theta_d \quad (\text{A66b})$$

b. Limit of small dendritic threshold

As shown in the main text numerically and above for $\alpha < \alpha_c$, in the low dendritic threshold regime for fixed θ_s , the model with Polsky and ReLU activation function behaves like a one-layer model. We give another quantitative argument here for $\alpha = \alpha_c$. Since $\theta_d \rightarrow 0$ the right-hand side of the first of (A64) should go to zero. Since the function $G(B) - BH(B)$ does not go to zero for finite values of B , by necessity $C \rightarrow 0$. By the last of (A64), this requires $\Gamma_0 \rightarrow 0$, i.e. $Q \rightarrow 0$. In this limit we get

$$\Gamma_0 = \Delta_Q - \Delta_0 \simeq \Gamma_1 Q, \quad (\text{A67})$$

which holds in the perceptron case. The saddle point equations therefore become equivalent to the one found in the perceptron.

6. Distribution of synaptic weights

The distribution of synaptic weights is:

$$P(W) = \left\langle \left\langle \frac{1}{\Omega} \int_0^\infty \prod_{li} dW_{li} \prod_{\mu=1}^{\alpha N} \Theta \left[\frac{\sigma^\mu}{\sqrt{K}} \left(\sum_{l=1}^K c_l g \left(\sqrt{\frac{K}{N}} \sum_{i=1}^{N/K} W_{li} \xi_{li}^\mu - \sqrt{\frac{N}{K}} \theta_d \right) - K\theta_s \right) - \kappa \right] \delta(W - W_{11}) \right\rangle \right\rangle_{\{\xi^\mu, \sigma^\mu\}} \quad (\text{A68})$$

with respect to the first weight of the first sub-perceptron W_{11} for simplicity. Resorting to the replica method by introducing n replicas we have:

$$P(W) = \lim_{n \rightarrow 0} \mathbb{E} \int_0^\infty \prod_{i,l,a} dW_{li}^a \int \prod_{\mu,a,l} \frac{d\lambda_{li}^a d\hat{\lambda}_{li}^a}{2\pi} e^{i\lambda_{li}^a \hat{\lambda}_{li}^a} \prod_{\mu=1}^{\alpha N} \Theta \left[\frac{\sigma^\mu}{\sqrt{K}} \left(\sum_l c_l g(\lambda_{li}^a) - K\theta_s \right) - \kappa \right] \delta(W - W_{11}) \times e^{i\sqrt{\frac{N}{K}} \theta_d \sum_{\mu,a,l} \hat{\lambda}_{li}^a} \prod_{l,i,\mu} \left\langle e^{-i\xi_{li}^\mu \sqrt{\frac{K}{N}} \sum_a W_{li}^a \lambda_{li}^a} \right\rangle_{\xi_{li}^\mu} \quad (\text{A69})$$

Repeating the same steps as in section A3 we have

$$P(W) = \lim_{n \rightarrow 0} \int \prod_{a<b,l} \frac{dq_l^{ab} d\hat{q}_l^{ab}}{2\pi K/N} \int \prod_{a,l} \frac{dQ_l^a d\hat{Q}_l^a}{2\pi K/N} \int \prod_{a,l} \frac{dM_l^a d\hat{M}_l^a}{2\pi \sqrt{K/N}} e^{-\frac{N}{K} \sum_{a<b,l} q_l^{ab} \hat{q}_l^{ab} - \frac{N}{K} \sum_{a,l} Q_l^a \hat{Q}_l^a - \frac{N}{K} \bar{W} \sum_{a,l} \hat{M}_l^a} \times e^{N\alpha G_E(q_l^{ab}, Q_l^a, M_l^a) + (\frac{N}{K} - 1) G_S(\hat{q}_l^{ab}, \hat{Q}_l^a, \hat{M}_l^a)} \int_0^\infty \prod_{l,a} dW_l^a \delta(W - W_1) e^{\sum_{a<b,l} \hat{q}_l^{ab} W_l^a W_l^b + \sum_{a,l} \hat{Q}_l^a (W_l^a)^2 + \sum_{a,l} \hat{M}_l^a W_l^a} \quad (\text{A70})$$

where the entropic and energetic terms are the same as in Eqs. (A14a), (A14b) and the order parameters are those defined in (A11). In the limit $n \rightarrow 0$ therefore

$$P(W) = \lim_{n \rightarrow 0} \int_0^\infty \prod_{l,a} dW_l^a \delta(W - W_1) e^{\sum_{a<b,l} \hat{q}_l^{ab} W_l^a W_l^b + \sum_{a,l} \hat{Q}_l^a (W_l^a)^2 + \sum_{a,l} \hat{M}_l^a W_l^a} \quad (\text{A71})$$

provided the order parameters satisfy the same saddle point equations as before. Under the RS ansatz expression (A71) becomes:

$$P(W) = \Theta(W) \int Dz \frac{e^{-\frac{1}{2}(\hat{q} - 2\hat{Q})W^2 + (\sqrt{\hat{q}}z + \hat{M})W}}{\int_0^\infty dW e^{-\frac{1}{2}(\hat{q} - 2\hat{Q})W^2 + (\sqrt{\hat{q}}z + \hat{M})W}} = \Theta(W) \sqrt{\hat{q} - 2\hat{Q}} e^{-\frac{1}{2}(\hat{q} - 2\hat{Q})W^2 + \hat{M}W} \int Dz e^{\sqrt{\hat{q}}Wz} \frac{G\left(-\frac{\sqrt{\hat{q}}z + \hat{M}}{\sqrt{\hat{q} - 2\hat{Q}}}\right)}{H\left(-\frac{\sqrt{\hat{q}}z + \hat{M}}{\sqrt{\hat{q} - 2\hat{Q}}}\right)} \quad (\text{A72})$$

Notice that the dependence of $P(W)$ on K and on the activation function is not explicit, but is concealed inside the order parameters that clearly depend on them through the saddle point they have to satisfy. Notice also that for $\alpha = 0$ the synaptic weight satisfies an exponential distribution

$$P(W) = \Theta(W) \hat{M} e^{-\hat{M}W} = \Theta(W) \frac{f_{\text{in}}}{\theta_d} e^{-\frac{f_{\text{in}}}{\theta_d} W} \quad (\text{A73})$$

This is to be expected, since at $\alpha = 0$ the only constrain that is required apart for the fact that the synapses are non-negative, is that their average is $\bar{W} = \frac{\theta_d}{f_{\text{in}}}$.

a. Distribution of synaptic weights in the maximal storage limit

In the critical capacity limit $\alpha \rightarrow \alpha_c$ the expression of the distribution of synaptic weight greatly simplifies. Using the scalings in (A54) we find

$$P(W) = \Theta(W) e^{-\frac{A}{2dq} W^2 - \frac{B\sqrt{C}}{dq} W} \sqrt{\frac{A}{dq}} \int Dz e^{\frac{\sqrt{C}}{dq} Wz} \left[G \left(\sqrt{\frac{C}{A}} \frac{z - B}{\sqrt{\hat{q} - 2\hat{Q}}} \right) \Theta(z - B) - \sqrt{\frac{C}{Adq}} (z - B) \Theta(B - z) \right] \quad (\text{A74})$$

Using the identity

$$\int Dz e^{az} (z + b) \Theta(-b - z) = (a + b) e^{\frac{a^2}{2}} H(a + b) - e^{-ab} G(b) \quad (\text{A75})$$

we obtain

$$P(W) = H(-B) \delta(W) + \frac{1}{\sqrt{2\pi}W_\star} e^{-\frac{(W+BW_\star)^2}{2W_\star^2}} \Theta(W) \quad (\text{A76})$$

where $W_\star \equiv \frac{\sqrt{C}}{A}$. As showed in [38] in the one layer neuron model the synaptic weight distribution changes from being exponential to being a Gaussian plus a spike consisting to a fraction $H(-B)$ of “silent” weights at the critical capacity. Indeed as constraints due to the training set are added, more and more synapses tend to assume low weight. This is the case also in our two layer neuron model. It is interesting to note that both the distribution of synaptic weight at finite α (A72) and at critical capacity are in form exactly the same as the one derived in [38] for the one layer neuron model; the dependence on the non-linearity induced by the dendrites is actually implicit in the order parameters.

In Fig. 2 we show how the fraction of silent synapses $p_0 = H(-B)$ depends on the somatic threshold for the ReLU, ReLU-Sat and Polsky non-linearities. We also show in the Polsky case, how p_0 depends on the parameters defining the shape of the function itself, x_{min} and γ .

Appendix B: Numerical experiments

1. Choice of the thresholds

In this section, we outline a possible selection of thresholds θ_d and θ_s , that can be utilized in numerical experiments and in the comparison with the analytical results. For SGD and the non-linear neuron case, as described in equation (A2), the first threshold θ_d is chosen to ensure that the pre-activations are distributed within the active range of the non-linear transfer function at initialization. The second threshold, θ_s , is selected to maintain consistency between the output coding level and the ground-truth coding level. In contrast, for the linear neuron (perceptron) case, only a single threshold θ is involved, which determines the mean of the weights. By applying a suitable rescaling, this threshold can be arbitrarily fixed, while the cross-entropy parameter γ_{ce} and the learning rate ζ must be appropriately chosen.

To achieve the desired output coding level f_{out} during the initial forward pass, two factors have to be considered:

1. The distribution of pre-activations incoming to the hidden units, in order to choose the first threshold θ_d .

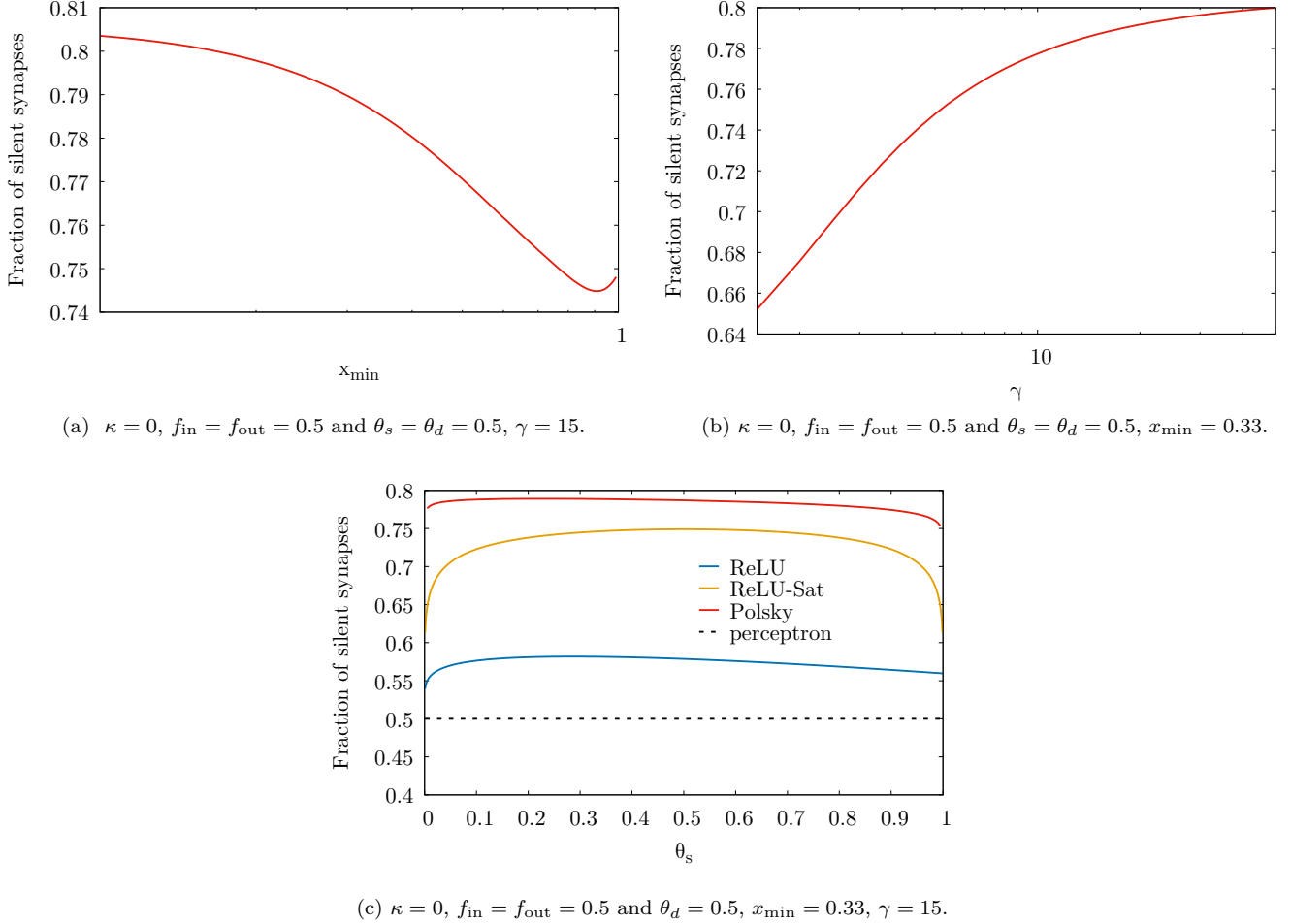


Figure 11. In the top panels we plot the fraction of silent synapses for the Polsky non-linearity as a function the parameters x_{min} and γ . The bottom panel shows the fraction of silent synapses as a function of the somatic threshold, comparing the ReLU, the “saturating” ReLU and Polsky non-linearity when no robustness parameter κ is imposed. The dashed black line represents the case of the one-layer neuron model, where the critical capacity $\alpha_c^{\text{perc}} = 1$. In the captions of the panels we show the value of the fixed external parameters.

2. The probability of generating either 1 or 0 after applying the Heaviside function to the neuron output. This probability is determined by the value of θ_d and the specific functional form of the non-linearity applied to the hidden units. By selecting the second threshold θ_s based on these factors, we can achieve the desired output coding level.

Considering random weights W , the pre-activations incoming to the hidden units for a given pattern ξ are computed as follows:

$$a = \sqrt{\frac{K}{N}} \sum_i W_i \xi_i \quad (\text{B1})$$

In the limit where $N, K \rightarrow \infty$ and $\frac{N}{K} \rightarrow \infty$, the distribution of these pre-activations converges to a Gaussian distribution by the central limit theorem (CLT). The mean μ and variance σ^2 of this Gaussian distribution depend on the input coding level f_{in} , the dendritic threshold θ_d , and the initial weight distribution, which we assume to be uniform for simplicity. In our analysis, we consider the first threshold θ_d to be of order 1 ($\theta_d \sim O(1)$), and the weights W_i are randomly drawn from a uniform distribution in the range $[0, W_M]$, where W_M is also of order 1 ($W_M \sim O(1)$).

The mean and variance of the i.i.d. variables ξ_i and W_i are given by:

$$\mathbb{E}[\xi_i] = f_{\text{in}} \quad (\text{B2})$$

$$\text{Var}[\xi_i] = f_{\text{in}}(1 - f_{\text{in}}) \quad (\text{B3})$$

$$\mathbb{E}[W_i] = \frac{W_M}{2} \quad (\text{B4})$$

$$\text{Var}[W_i] = \frac{W_M^2}{12} \quad (\text{B5})$$

Since ξ_i and W_i are both i.i.d., the mean and variance of their product can be computed using the following properties:

$$\mathbb{E}[\xi_i W_i] = \mathbb{E}[\xi_i] \mathbb{E}[W_i] = f_{\text{in}} \frac{W_M}{2} \quad (\text{B6})$$

$$\text{Var}[\xi_i W_i] = (\text{Var}[\xi_i] + \mathbb{E}^2[\xi_i])(\text{Var}[W_i] + \mathbb{E}^2[W_i]) - \mathbb{E}^2[\xi_i] \mathbb{E}^2[W_i] \quad (\text{B7})$$

$$= \text{Var}[\xi_i](\text{Var}[W_i] + \mathbb{E}^2[W_i]) + \text{Var}[W_i] \mathbb{E}^2[\xi_i] \quad (\text{B8})$$

$$= f_{\text{in}}(1 - f_{\text{in}}) \left(\frac{W_M^2}{12} + \frac{W_M^2}{4} \right) + \frac{W_M^2}{12} f_{\text{in}}^2 \quad (\text{B9})$$

$$= \frac{1}{12} (4 - 3f_{\text{in}}) f_{\text{in}} W_M^2 \quad (\text{B10})$$

To estimate the mean and standard deviation of the pre-activations incoming to the hidden units (B1), we can apply the central limit theorem (CLT) to the sum of the products $\xi_i W_i$:

$$\mathbb{E}[a] = \mathbb{E} \left[\sqrt{\frac{K}{N}} \sum_{i=1}^{N/K} \xi_i W_i \right] = \sqrt{\frac{K}{N}} \sum_{i=1}^{N/K} \mathbb{E}[\xi_i W_i] = \sqrt{\frac{N}{K}} f_{\text{in}} \frac{W_M}{2} \quad (\text{B11})$$

$$\text{Var}[a] = \text{Var} \left[\sqrt{\frac{K}{N}} \sum_{i=1}^{N/K} \xi_i W_i \right] = \frac{K}{N} \sum_{i=1}^{N/K} \text{Var}[\xi_i W_i] = \frac{1}{12} (4 - 3f_{\text{in}}) f_{\text{in}} W_M^2 \quad (\text{B12})$$

The mean of the Gaussian distribution of the preactivations is:

$$\mu = \mathbb{E}[a] - \theta_d \sqrt{\frac{N}{K}} = \sqrt{\frac{N}{K}} f_{\text{in}} \frac{w_M}{2} - \theta_d \sqrt{\frac{N}{K}} \quad (\text{B13})$$

It is reasonable (given the form of the transfer functions we consider) to center the Gaussian distribution of the pre-activations around 0, so that $\mu = 0$ and from (B13) we obtain:

$$W_M = \frac{2\theta_d}{f_{\text{in}}} \quad (\text{B14})$$

that self-consistently gives $W_M \sim O(1)$ if $\theta_d \sim O(1)$.

The standard deviation of the Gaussian distribution of the pre-activations is:

$$\sigma = \sqrt{\text{Var}[a]} = \frac{W_M}{2} \sqrt{\frac{1}{3} (4 - 3f_{\text{in}}) f_{\text{in}}} \quad (\text{B15})$$

We can treat the standard deviation σ as a parameter and solve for the first threshold θ_d :

$$\theta_d = \sigma \sqrt{\frac{3f_{\text{in}}}{(4 - 3f_{\text{in}})}}. \quad (\text{B16})$$

For example with $f_{\text{in}} = 0.5$ and by choosing $\sigma = 1$ for the Polsky transfer function we find $\theta_d = 0.775$. After determining the value of θ_d , we can proceed to fix θ_s . Let $h_k = g(a_k)$ denote the activations of the hidden units, where g is the transfer function and a_k is the pre-activation signal arriving at the dendritic unit k . Our goal is to estimate the probability of generating a 1 in the neuron's final output and ensure that it is equal to f_{out} , thereby preserving the output coding level on average. Given the application of a Heaviside transfer function to the output, this probability can be expressed as:

$$p(\text{out} = 1) = p \left(\frac{1}{K} \sum_{k=1}^K h_k > \theta_s \right) \quad (\text{B17})$$

$$= 1 - F_{\mathcal{N}(\mu_2, \sigma_2^2)}(\theta_s) = f_{\text{out}} \quad (\text{B18})$$

where F is the cumulative density function, and in (B18), we applied the CLT once more, which ensures that the output preactivations follow a Gaussian distribution with mean μ_2 and standard deviation σ_2 , implicitly dependent on the transfer function applied to the hidden units and their preactivation distribution.

It is therefore possible to find θ_s by solving the equation:

$$F_{\mathcal{N}(\mu_2, \sigma_2^2)}(\theta_s) = 1 - f_{\text{out}}. \quad (\text{B19})$$

To define the values of μ_2 and σ_2 , we denote the hidden unit activations by $h_k = g(a_k)$ and recall that we imposed $P(a_k) = \mathcal{N}_{0,1}(a_k)$ when calculating the first threshold θ_d . The CLT can also be applied to the activations h_k , yielding $P\left(\frac{1}{K} \sum_{k=1}^K h_k\right) = \mathcal{N}_{\mu_h, \sigma_h^2}$, where μ_h and σ_h^2 are the mean and variance of h_k , respectively. These values can be calculated for the Pinsky transfer function as follows

$$\mathbb{E}[h_k] = \int_{-\infty}^{\infty} g(x) \mathcal{N}_{(0,1)}(x) dx = 0.369 \quad (\text{B20})$$

$$\text{Var}[h_k] = \int_{-\infty}^{\infty} g^2(x) \mathcal{N}_{(0,1)}(x) dx - E^2[h_k] = 0.202 \quad (\text{B21})$$

We see that for $f_{\text{out}} = 0.5$ we can simply impose:

$$\mathbb{E}[h_k] = \theta_s \quad (\text{B22})$$

For Pinsky transfer functions applied to the hidden units, we can numerically evaluate (B20), yielding $\theta_s = \mathbb{E}[h_k] = 0.369$.

Another notable case is that of Heaviside transfer functions, where $\mathbb{E}[h_k] = 0.5$. In this scenario, we can employ a simpler argument to estimate the thresholds: since the output of the hidden units is independent of θ_d , the only free parameter is θ_s . We have² $p\left(\sum_{k=1}^K h_k > K\theta_s\right) = 1 - \theta_s$. By imposing $1 - \theta_s = f_{\text{out}}$, we obtain $\theta_s = 1 - f_{\text{out}}$, which, for $f_{\text{out}} = 0.5$, is equivalent to (B22).

2. Choice and scaling of the hyper-parameters

Consider the transfer function implemented by the neuron with non-linear dendritic branches, which represents the output preactivation prior to the thresholding operation performed by the Θ -function:

$$\Delta_{\text{out}}^\mu = \frac{1}{\sqrt{K}} \sum_{l=1}^K c_l g\left(\sqrt{\frac{K}{N}} \sum_{i=1}^{N/K} W_{li} \xi_{li}^\mu - \sqrt{\frac{N}{K}} \theta_d\right) - \sqrt{K} \theta_s \quad (\text{B23})$$

we impose that $W \in \left[0, \frac{2\theta_d}{f_{in}}\right]$ and consequently:

$$W \sim O\left(\frac{\theta_d}{f_{in}}\right).$$

If we assume that: $\theta_d \sim O(1)$, and $\theta_s \sim O(1)$ we have: $W \sim O\left(\frac{1}{f_{in}}\right)$.

We also have: $\sum_{i=1}^{N/K} W_{li} \xi_{li}^\mu \sim O\left(\frac{N}{K}\right)$. Consequently, from (B23), we observe that the dendritic pre-activations scale as:

$$\left(\sqrt{\frac{K}{N}} \sum_{i=1}^{N/K} W_{li} \xi_{li}^\mu - \sqrt{\frac{N}{K}} \theta_d\right) \sim O\left(\sqrt{\frac{N}{K}}\right). \quad (\text{B24})$$

² The probability of generating a 1 in the output is $\frac{\theta_s}{K}$. To preserve the output coding level, we set $\theta_s = K(1 - f_{\text{out}})$.

Consequently, the pre-activation variance remains finite in the limit $N \rightarrow \infty$, which is the primary motivation for choosing these scalings, as the pre-activation variance is a crucial factor in ensuring the consistency of the learning setting when varying the input dimensionality N and the number of dendritic branches K .

Applying the same type of consideration to the pre-activation of the single output node in (B23) and recalling that $c_l = 1 \forall l$ and $g(\cdot) \sim O(1)$, we find that it scales as:

$$\Delta_{\text{out}}^\mu \sim O\left(\theta_s \sqrt{K}\right) \quad (\text{B25})$$

Least-action learning algorithm (LAL) In the LAL algorithm, when a wrong prediction occurs for a specific pattern, we identify the neurons that contribute to the error, i.e., the neurons at positions l_* that have negative values for the following local stability measure over the dendritic branches:

$$\delta_l^\mu = -\sigma^\mu \left(\sqrt{\frac{K}{N}} \sum_{i=1}^{N/K} W_{li} \xi_{li}^\mu - \sqrt{\frac{N}{K}} \theta_d \right) \quad (\text{B26})$$

and then we proceed to updating the weights with the following (possibly stochastic) rule:

$$w_{il_*} \leftarrow w_{il_*} + \zeta \sigma^\mu \xi_{il_*}^\mu \quad (\text{B27})$$

By requiring an update of the same order as the weights, i.e., $w \sim O(\theta_d) \implies \zeta \sigma^\mu \xi_{il_*}^\mu \sim O(\theta_d)$, we obtain the desired scaling for the learning rate ζ :

$$\zeta \sim O\left(\frac{\theta_d}{f_{in}}\right) \quad (\text{B28})$$

Stochastic Gradient Descent (SGD) with cross-entropy loss Recalling the expression for the cross-entropy loss used to investigate the performance of stochastic gradient descent (SGD) on the neuron:

$$\mathcal{L}_{ce}(\Delta_{\text{out}}^\mu) = \frac{1}{2\gamma_{ce}} \log(1 + \exp(-2\gamma_{ce}\Delta_{\text{out}}^\mu)) \quad (\text{B29})$$

we can estimate the gradients of the cross-entropy loss, which are used in the SGD update, as follows:

$$\frac{\partial \mathcal{L}_{ce}(\Delta)}{\partial \Delta} = -\frac{1}{1 + \exp(2\gamma_{ce}\Delta)} \quad (\text{B30})$$

$$\sim O(1) \quad (\text{B31})$$

where the last step holds (due to (B25)) if:

$$\gamma_{ce} \sim O\left(\frac{1}{\theta_s \sqrt{K}}\right). \quad (\text{B32})$$

Proceeding with the derivative w.r.t. to the weights, we obtain:

$$\frac{\partial \mathcal{L}_{ce}(\Delta(W))}{\partial W} = \frac{\partial \Delta(W)}{\partial W} \frac{\partial \mathcal{L}_{ce}(\Delta)}{\partial \Delta} \quad (\text{B33})$$

$$= \frac{\partial}{\partial W} \left(\frac{1}{\sqrt{K}} \sum_{l=1}^K c_l g \left(\sqrt{\frac{K}{N}} \sum_{i=1}^{N/K} W_{li} \xi_{li}^\mu - \sqrt{\frac{N}{K}} \theta_d \right) - \sqrt{K} \theta_s \right) \frac{\partial \mathcal{L}_{ce}(\Delta)}{\partial \Delta} \quad (\text{B34})$$

$$= \left[\frac{1}{\sqrt{K}} \sum_{l=1}^K \left(c_l g' \left(\sqrt{\frac{K}{N}} \sum_{i=1}^{N/K} W_{li} \xi_{li}^\mu - \sqrt{\frac{N}{K}} \theta_d \right) \sqrt{\frac{K}{N}} \sum_{i=1}^{N/K} \xi_{li}^\mu \right) \right] \frac{\partial \mathcal{L}_{ce}(\Delta)}{\partial \Delta} \quad (\text{B35})$$

$$\sim O\left(\frac{1}{\sqrt{K}} \sqrt{\frac{K}{N}} f_{in} N\right) O(1) \quad (\text{B36})$$

$$\sim O(f_{in} \sqrt{N}) \quad (\text{B37})$$

where in the penultimate step, we have used the fact that the derivative of the function g is bounded within the interval $[0, 1]$ so that $g'(\cdot) \sim O(1)$; that $\sum_{i=1}^{N/K} \xi_{il}^\mu \sim O(f_{in} \frac{N}{K})$; and (B31).

At this point, recalling that the SGD update rule is:

$$w_{il} \leftarrow w_{il} - \zeta \nabla_{w_{il}} \mathcal{L}(w_{il}) \quad (\text{B38})$$

and imposing an update of the same order as the weights, i.e., $w \sim O(\theta_d) \implies \zeta \nabla_w \mathcal{L}(w) \sim O(\theta_d)$, we find the desired scaling for the learning rate ζ :

$$\zeta \sim O\left(\frac{\theta_d}{f_{in} \sqrt{N}}\right) \quad (\text{B39})$$

Comparison between the dendritic and the linear neuron The transfer function of the linear neuron (i.e. the perceptron model), is given by:

$$\Delta_{\text{perc, out}}^\mu = \frac{1}{\sqrt{N}} \sum_{i=1}^N W_i \xi_i^\mu - \sqrt{N} \theta_s. \quad (\text{B40})$$

From this expression, and observing that the weights scale with θ_s , we obtain the following scalings for the learning rate ζ and cross-entropy parameter γ_{ce} :

$$\zeta_{LAL} \sim O\left(\frac{\theta_s}{f_{in}}\right), \quad \zeta_{SGD} \sim O\left(\frac{\theta_s}{f_{in} \sqrt{N}}\right), \quad \gamma_{ce} \sim O\left(\frac{1}{\theta_s \sqrt{N}}\right). \quad (\text{B41})$$